ABSTRACT

Title of Document: DESIGN AND EXPERIMENTATION OF A MANUFACTURABLE SOLID DESICCANT WHEEL ASSISTED SEPARATE SENSIBLE AND LATENT COOLING PACKAGED TERMINAL AIR CONDITIONING SYSTEM

Michael Vincent Cristiano, Master of Science, 2014

Directed By: Research Professor Yunho Hwang, Mechanical Engineering

Packaged terminal air conditioning (PTAC) systems are typically utilized for space heating and cooling in hotels and apartment buildings. However, in an effort to reach comfortable relative humidity in the conditioned space, they cool the air to its dew point and some reheating may be required to reach room set point temperature. In this study a commercial prototype of a solid desiccant wheel assisted separate sensible and latent cooling (SSLC) packaged terminal air conditioning (PTAC) system was designed . This iteration of the SSLC prototype was modeled based on PTAC type air conditioning units and was designed to achieve a 30% increase in system efficiency over current commercially available PTAC units. Heat exchangers used as evaporator and condenser were modeled in Coildesigner and VapCyc was used for system level modeling. Also a test facility was constructed in order to evaluate the performance of the proposed SSLC unit. Shakedown testing was conducted under

various operating conditions in order to compare the SSLC system to a standard PTAC unit without desiccant wheel. With the necessary adjustments to the experimental prototype, the system could increase the overall capacity through latent cooling with negligible additional power consumption.

DESIGN AND EXPERIMENTATION OF A MANUFACTURABLE SOLID DESICCANT WHEEL ASSISTED SEPARATE SENSIBLE AND LATENT COOLING PACKAGED TERMINAL AIR CONDITIONING SYSTEM

By

Michael Vincent Cristiano

Thesis submitted to the Faculty of the Graduate School of the
University of Maryland, College Park, in partial fulfillment
of the requirements for the degree of
Master of Science
2014

Advisory Committee:

Research Professor Yunho Hwang, Chair
Assistant Professor Amir Riaz
Associate Professor Bao Yang

Acknowledgements

I would like to thanks everyone who had a hand in making the completion of my graduate degree possible in such a short amount of time. I am extremely grateful for the work others put in to ensure my work would be completed by the time I needed to move on to my next naval assignment. First I would like to thank Dr. Reinhard Radermacher and Dr. Yunho Hwang for allowing me the opportunity to become a part of CEEE. I would especially like to thank Dr. Hwang as my advisor throughout the entire process and helping me be successful in completing my work.

I would also like to thank Jan Muehlbauer who provided me with the skills necessary to construct my experimental setup, as well as guide me throughout the entire process whenever assistance was necessary. Coming into graduate school with no lab experience was made easier through the assistance of Jan in the lab. In addition, I would like to thank Dr. Jiazhen Ling who assisted me in the project from the begin, setting me on the right foot and always available to help me out when beginning the project.

I would like to especially thank Sahil Popli as well as all of the other graduate students who helped me along the way. Sahil assisted me and gave me guidance whenever necessary, no matter how busy he was and no matter the time of day. Without Sahil, I would not have made it as far as I did in my time at the University of Maryland.

Additionally, I would like to thank my family and friends who have supported me from the beginning, and especially during the stressful short amount of time spent completing my graduate degree. Finally, I would like to thank my girlfriend Jane

who none of this would be possible without. Jane has supported me during my entire time at the University of Maryland while pursuing her own education while also working and I could not be more grateful that she is in my life.

Table of Contents

List of Tables

List of Figures

Nomenclature

Abbreviations:

AC	Air Conditioning	
AHU	Air Handling Unit	
CAD	Computer Aided Design	
COP	Coefficient of Performance	
c_p	Specific Heat Capacity	[kJ-kg-K]
DAQ	Data Acquisition	
DW	Desiccant Wheel	
EES	Engineering Equation Solver	
EXV	Electronic Expansion Valve	
h	Enthalpy	[kJ/kg]
MCHX	Micro Channel Heat Exchanger	
m	Mass Flow Rate	[kg/s]
P	Pressure	[kPa]
PR	Pressure Ratio	
PTAC	Package Terminal Air Conditioner	
Q	Capacity	[kW]
RH	Relative Humidity	[%]
RPM	Revolutions Per Minute	
s	Entropy	[kJ/kg-K]
SHF	Sensible Heat Factor	
SSLC	Separate Sensible and Latent Cooling	
T	Temperature	[°C]

ΔT	Evaporator Inlet Temperature Difference	[K]
VCC	Vapor Compression Cycle	
VCS	Vapor Compression System	
V_{disp}	Compressor Displacement Volume	[m^3/rev]
$\dot{W}$	Power	[kW]

Greek Symbols:

η	Compressor Efficiency	
ρ	Density	[kg/m^3]
ω	Humidity Ratio	[$kg_{water\ vapor}/kg_{dryair}$]

Subscripts:

a	air
amb	ambient
comp	compressor
comp, in	compressor inlet
comp, out	compressor outlet
cond	condenser
drop, cond	condenser pressure drop
drop, evap	evaporator pressure drop
evap	evaporator
evap, in	evaporator inlet
isen	isentropic

sat	saturation
v	vapor
vol	volumetric
w	water

Chapter 1: Introduction

1.1: Separate Sensible and Latent Cooling (SSLC)

Separate sensible and latent cooling methods are the next step in cooling technologies. The vapor compression cycle (VCC) today boasts a Coefficient of performance (COP) of around 3, but with SSLC systems, COP's closer to 3.8-4.0 can be attained. Cooling can be broken into two parts: sensible cooling and latent cooling. Sensible cooling is the reduction in temperature whereas latent cooling is the removal of humidity, or moisture from the air. Standard vapor compression systems (VCS) often overcool the space air to reach the dew point temperature, or the temperature at which moisture from the air will condense to lower the humidity ratio of the air. This overcooling requires a greater pressure difference between the high- and low-side pressures of the VCC, requiring a greater compressor power input.

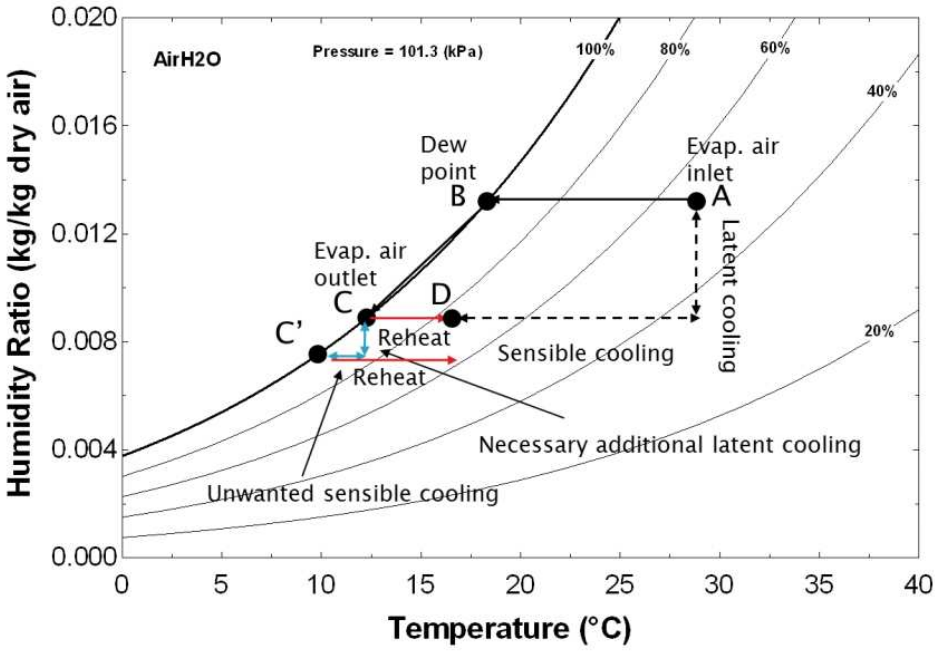

Figure 1: Psychrometric process for conventional VCC [1]

Figure 1 shows the psychrometric process of a standard VCS. The air is cooled across the evaporator, passing through point B to begin the latent cooling to point C. Point D is the target condition, which in some cases requires reheating of the air to meet the specified air temperature. The reheating could also account for additional power consumption.

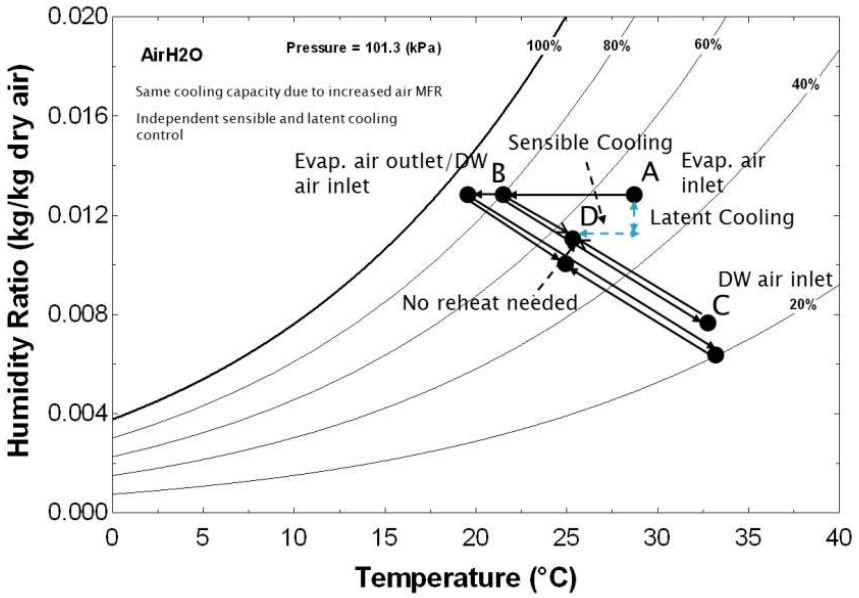

Figure 2: Psychrometric process of SSLC System [1]

Figure 2 shows the psychrometric process of one type of SSLC system. In this case, air is cooled over the evaporator slightly below the target point D to point B. The air is only slightly overcooled because the process used to remove the moisture from the air increases the temperature, but does not affect the overall efficiency of the system substantially. The specified temperature and humidity level can be achieved through two separate processes with less energy consumption. No substantial overcooling occurs, reducing the compressor power input, and no additional reheating is required, eliminating that power consumption altogether.

Specifically, the SSLC system used in this investigation is the integrated solid desiccant wheel (DW) and VCS. A standard vapor compression system (VCS) removes heat from a space by flowing air over a cold evaporator, and exhausting the heat to the environment by flowing air over the warm condenser. The solid DW-VCS

operates similarly, with an additional state point in the process air flow and an additional waste heat air flow path.

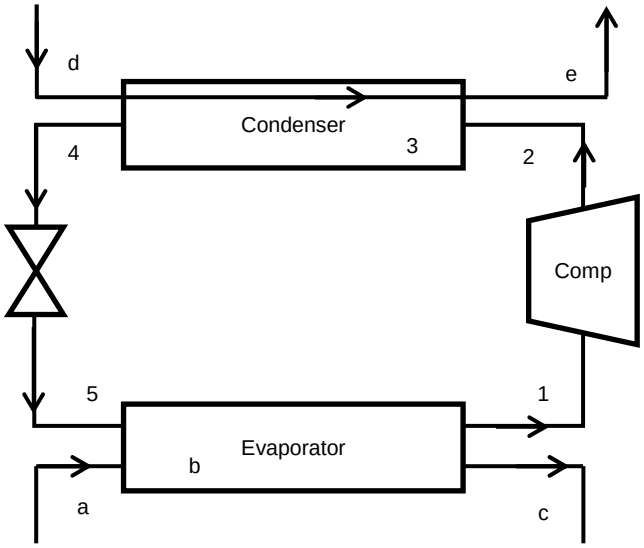

Figure 3: Standard Vapor Compression Cycle

Figure 3 shows the standard five state points VCC. Although desuperheating occurs within the condenser as an entire process from state point 2 to state point 4, the division is shown to show the difference in Figure 4. This cycle has three loops; the refrigeration loop, the process air loop over the evaporator and the exhaust air loop over the condenser. Process a-b-c is also divided out because the air is reduced in temperature from a-b, and then reduced in temperature and humidity in b-c.

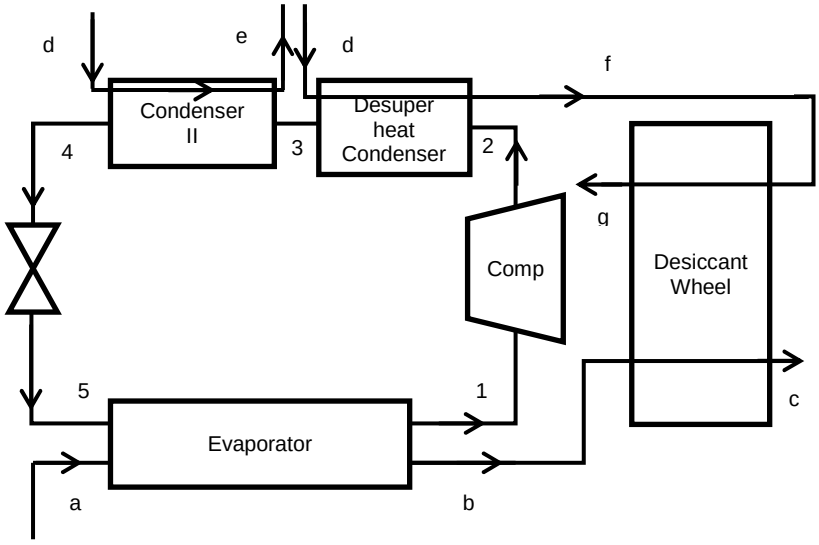

Figure 4: Integrated Solid DW-Vapor Compression Cycle

Figure 4 shows the integrated DW-VCC. In the integrated system, there are four loops. The refrigeration loop remains the same, with the addition of an extra condenser, appropriately named as the desuperheat condenser. The desuperheat condenser is specifically designed to remove heat only until the point where the refrigerant crosses from the superheated vapor region into the two-phase region.

The purpose of this extra condenser is to ensure that the air is heated to the required regeneration temperature of the DW. The DW removes moisture from the process air loop, but in order to remove moisture absorbed in the DW, hot dryer air must pass through the DW on the regeneration side. This extra condenser has the added benefit of reutilizing what would normally be considered waste heat, whereas a standard solid DW system would usually utilize an extra electric heater, consuming even more energy.

The process air side loop separates the sensible and latent cooling between the evaporator and the DW, respectively. Because the evaporator is no longer required to

remove the latent load, the evaporation temperature can be much closer to the target space temperature.

Finally, the exhaust loop remains the same, but does not require as large of a capacity condenser because part of the load was removed through the desuperheat condenser. The remaining heat load is exhausted to the environment at a lower temperature.

Not only does separate sensible and latent cooling increase COP and reduce power consumption, it also increases thermal comfort. It is rare to see a more efficient system that does not come at the cost of comfort or luxury. A person's humidity comfort level can be specifically met without reducing the temperature to uncomfortable levels. SSLC units give the user more precise control over their comfort while also saving energy.

1.2: Packaged Terminal Air Conditioning (PTAC) Unit

The packaged terminal air conditioner (PTAC) is a relatively small self-contained air handling unit primarily used in hotels, small office spaces and some apartment and residential areas. The PTAC unit sits in the wall. All heat and mass transfers occur either through the front or back of the unit. The space air is conditioned and returned to the space through the front of the unit, and heat is exhausted from the condensers in the VCS through the back of the unit as shown in Figure 5.

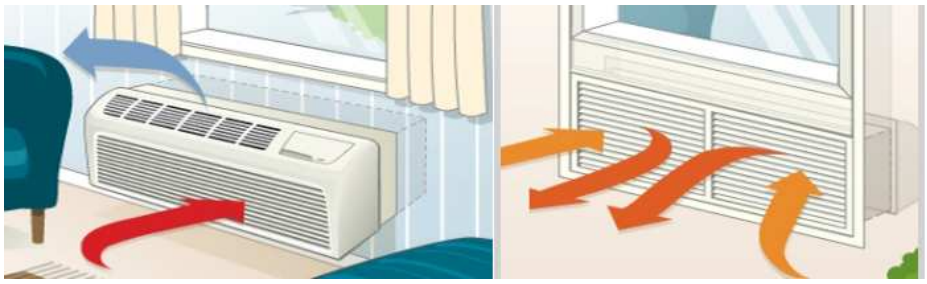

Figure 5: PTAC Unit Air Flow

The PTAC unit is large enough to fit the necessary additional components of a solid DW assisted AC system, unlike a standard window mounted AC unit. The PTAC unit is also the smallest sized air conditioner capable of fitting the additional components, which means that any AC unit larger than a PTAC unit could incorporate the DW assisted SSLC design.

1.3: Potential for Improvement

Based on previous experimentation run on the first prototype of the DW assisted SSLC unit, the design has the potential for a 30% increase in efficiency, or a COP of approximately 3.8 [2].

Table 1: Annual Cost and Savings for a 12,000 BTU PTAC Unit

	Annual Average Electricity Cost By State			
	Idaho (Low)	National Average	Connecticut (High)	Hawaii (Outlier High)
Electricity Rate [cent/kWhr]	6.44	9.9	16.35	31.59
PTAC Unit Cost [$]	749.99	749.99	749.99	749.99
SSLC Unit Cost [$]	900	900	900	900
Annual Estimated Operating Cost of PTAC* [$]	84.62	130.09	214.84	415.09
Annual Estimated Operating Cost of SSLC** [$]	67.62	103.95	171.68	331.70
Annual Savings Comparison (PTAC and SSLC) [$]***	17.00	26.14	43.16	83.40
Simple Payback Period [yrs]	8.82	5.74	3.48	1.80

***Power input 1.095 kW**

Table 1 shows a conservative estimate of the potential cost savings that come along with a unit 20% more expensive, but 30% more efficient. The annual estimated operating cost is based on an average cooling season of 1,200 hours. Most likely the cooling season will be much longer in regions where it is both hot and humid. Also, the SSLC system has the potential for greater than a 30% efficiency increase, especially over the course of an entire season, reducing the simple payback period to 2-5 years depending on the electricity cost and cooling season.

1.4: Objectives

The objectives of the current investigation can be broken down into the objectives of the entire project, and the design objectives that must be met in order for the design to meet product commercialization requirements.

1.4.1: Project Objectives

The project objects are as follows:

- Design and commercial PTAC prototype integrated with a solid DW.
- Experimentally investigate the effect of the DW assisted dehumidification on energy consumption and thermodynamic performance of the novel PTAC design.

1.4.2: Design Objectives

Based on discussion with the manufacturers and review of commercially available PTAC units, the following design objectives were considered for the design of the PTAC prototype in the current study:

- Restrict length and height to commercially available PTAC unit dimensions to allow retrofitting.
- Prototype unit's depth and weight to be less than 1.2 times commercially available PTAC unit dimensions
- Restrict cost to 1.2 times commercially available PTAC units of similar capacities
    - Approximately $900 for 12,000 BTU unit
    - Depending on region, simple payback period of 2-5 years
- Increase COP by approximately 30%

Chapter 2: Heat Exchanger and Cycle Modeling

Computer modeling and simulation of the system and its components were performed using several software packages including EES [3], CoilDesigner [4], and VapCyc [5]. EES stands for engineering equation solver and can be used to run state point analysis on thermodynamic models. EES uses a library of fluid and material properties along with input equations to model thermal systems. CoilDesigner is a steady-state simulation tool for determining individual heat exchanger performance based on inlet conditions and the geometry characteristics of the heat exchanger. VapCyc is a steady-state component-by-component simulation tool for modeling system performance based on directly calling CoilDesigner heat exchanger models as well as basic expansion device and compressor models [6],[7].

Modeling was first done for an air handling unit to determine the psychrometric state points of air and the sensible and latent cooling ratios of a standard cooling capacity. Then, based on the sensible cooling load, modeling was done for a standard VCC that operates above the dew point temperature of the process air, handling only the sensible load. The VCC model provided the required displacement of the compressor as well as the mass flow rate of the refrigerant.

Next, modeling was done using CoilDesigner to model each individual heat exchanger used, based on the heat exchangers in the preexisting PTAC unit. Finally, modeling of the entire system was done in VapCyc using the heat exchangers designed in CoilDesigner as well as the system properties determined in the EES models.

2.1: Cooling Load and VCC Model

The first step in modeling the system was to model a standard air handling unit to determine the sensible and latent cooling loads. Next, in order for the required sensible load to be met by the VCC a VCC was modeled. Both of these were done by using EES [3]. Equations used to represent both systems along with air and refrigeration properties built into EES make system modeling faster and more precise.

2.1.1: Psychrometric Process for Cooling and Dehumidification

The purpose of modeling the entire psychrometric process for cooling and dehumidification was two-fold. The first was to find the sensible heat factor (SHF), and the second was the water removal rate. The SHF is necessary to determine what percentage of cooling is sensible, which must be removed by a properly sized VCS, and what percentage is latent, which must be removed by a properly sized DW.

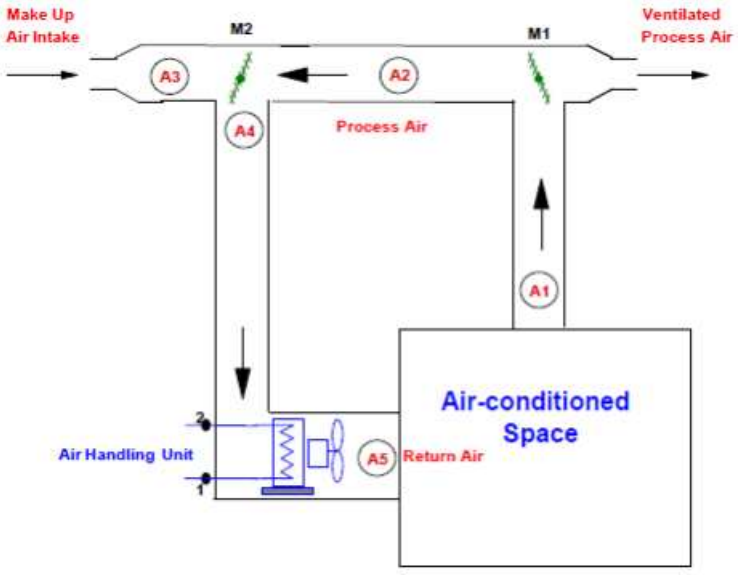

Figure 6: Air Handling Unit Process Diagram

Figure 6 shows the diagram of the entire system including the air handling unit. Beginning at state point [1], the air to be conditioned leaves the interior zone and flows through the system to junction M1 where a specified percentage of the air is reprocessed and the remaining air is ventilated out into the environment. Because, the air does not undergo any changes in humidity or temperature, state point [2] operates under the same condition as state point [1], a percentage of the total mass of the air. The temperature and relative humidity were set according to ANSI/AHRI Standard 310 [8]. Those two parameters can be used along with the constant pressure of 101.325 kPa to determine the rest of the parameters at state points [1] and [2] to include humidity ratio, wet bulb temperature, dew point temperature, enthalpy, density and specific volume.

At the junction M2, adiabatic mixing occurs between state point [2] and state point [3] with an output of state point [4]. State point [3] is air intake from outside represented by the ambient temperature and a set relative humidity. Using the temperature, relative humidity and pressure, the parameters of state point [3] could be determined as well.

In order to determine the parameters of state point [4], information from the surrounding state points in conjunction with adiabatic mixing relationships were used. The volumetric flow rate was assumed to be proportional to the required cooling load. The required cooling load could be set to any given size, but for the purpose of this analysis, in order to match similar units, a 12,000 BTU (3.5 kW) cooling load was set.

In order to determine the remaining parameters of the state points [4] and [5], equations relating the mass flow rates of the two state points needed to be

simultaneously solved using EES. First, it can be assumed that the mass flow rate of state points [4] and [5] are equal because there is only cooling and dehumidification occurring between the state points. Next, the adiabatic mixing occurring at junction M2 must be looked at again on mass and energy balances.

$$m_a[2] + m_a[3] = m_a[4] \quad (1)$$

$$\omega = \frac{m_v}{m_a} \quad (2)$$

$$m_a[2] * h[2] + m_a[3] * h[3] = m_a[4] * h[4] \quad (3)$$

$$m_a[2] * \omega[2] + m_a[3] * \omega[3] = m_a[4] * \omega[4] \quad (4)$$

Using the four governing equations relating to the adiabatic mixing at junction M2 along with the assumption that the mass flow rate between state points [4] and [5] stay constant, enough parameters at state points [4] and [5] can be determined in order to solve for the remaining parameters. The relative humidity and the humidity ratio were used at state point [5] to determine the rest of the parameters and the enthalpy and humidity ratio were used for state point [4]. At state point [5] the volumetric flow rate was used in addition to the specific volume in order to complete the analysis.

Next, the AHU's SHF and water removal rate were calculated. Between state points [4] and [5], cooling and dehumidification occur. The mass flow rate of the

excess water removed from the air during dehumidification, or the moisture removal rate was determined using the equation:

$$m_w = m_a[4] * (\omega[4] - \omega[5]) \quad (5)$$

During cooling and dehumidification, there is one inlet of moist air, and two outlets of water removed and dehumidified moist air. The cooling load can be calculated using mass flow rate and enthalpy. In order to determine the enthalpy of the water removed, the dew point temperature of state point [5] was used because that is the temperature at which the moisture from the air becomes liquid water. Along with the known pressure, the enthalpy was determined of the water. Then, the cooling load of the AHU was determined using the following equation.

$$m_a[4] * h[4] = Q_{cooling} + m_a[5] * h[5] + m_w * h_w \quad (6)$$

Because of the phase change occurring in the cooling and dehumidification process, the cooling can be broken down into sensible and latent cooling. The sensible cooling load can be found using:

$$Q_{sensible} = m_a * c_p(T[4] - T[5]) \quad (7)$$

The sensible cooling is the energy transferred through temperature change, without the energy change due to phase change. The sensible heat factor (SHF) was determined as the amount of sensible cooling to the total amount of cooling.

$$SHF = \frac{Q_{sensible}}{Q_{cooling}} \quad (8)$$

The latent load can then be determined by subtracting the sensible load from the total cooling load.

The model can be used to represent a system that exhausts air and vents in new air. For the purpose of the design, no ventilation or exhaust of the process air was included, making it a much simpler system. Increasing the percent vented and exhausted would overall increase both the sensible and latent loads due to the addition of ambient air from the environment. The results from the AHU model are shown in Table 2.

Table 2: Air Handling Unit Model Results

Parameter	Unit	Value
SHF	-	0.74
Moisture Removal Rate	g/s	0.365
Sensible Cooling Load	kW	2.58
Latent Cooling Load	kW	0.92
Total Cooling Load	kW	3.5

The SHF is usually around 70-75%. Based on the sensible cooling load, the VCS modeled next needs to be designed to handle around 2.58 kW of 100% sensible

cooling. The moisture removal rate is important later in determining the size of the DW based on material properties.

2.1.2: Vapor Compression Cycle

The VCC was modeled assuming a cooling capacity of 10,000 BTU (2.93 kW) in order to oversize the system by roughly 10%. First, a standard VCC model was developed, and then adjustments were made in order to achieve only sensible cooling and the COP's were compared.

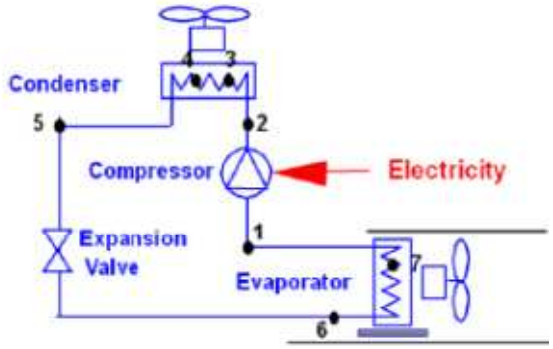

Figure 7: Vapor Compression Cycle Process Diagram

Figure 7 represents the VCC modeled. The first step was to set the conditions for the operation of the VCC.

Table 3 outlines the given parameters and equations initially set up to begin the analysis. These values were used in order to assume a more accurate model which would come closer to representing the actual overall system. The efficiencies and pressure drops model a more accurate assumption of what occurs in the system.

Table 3: Vapor Compression System Modeling Assumptions

Parameter	Value/Equation	Parameter	Value/Equation
T_{space} [°C]	27	η_{comp}	$\eta_{isen} * \eta_{motor}$
T_{amb} [°C]	35	$\Delta T_{evap,in}$ [K]	20
Q_{evap} [kW]	2.93	ΔT_{sat} [K]	10
RPM	3500	$T_{superheat}$ [°C]	10
η_{isen}	$0.9 - 0.0467 * PR$	$T_{subcooling}$ [°C]	5
η_{vol}	$1 - 0.04 * PR$	$P_{drop,evap}$ [kPa]	50
η_{motor}	0.95	$P_{drop,cond}$ [kPa]	100

The given temperatures, temperature differences and pressure drops were used to determine the parameters of each state point. The equations for the efficiencies could be used after solving for all of the state points in conjunction with the pressure ratio across the compressor (PR) as shown in the following equation.

$$PR = \frac{P_{comp,out}}{P_{comp,in}} \tag{9}$$

The system was broken up into seven state points. State point [1] was the superheated evaporator output as well as the compressor input. State point [2] was the compressor output and the condenser input. State point [3] was the point inside the condenser when the working fluid (R-410A) went from the superheated region to the two-phase region. State point [4] was the point in the cycle where the working fluid became a saturated vapor. State point [5] was the subcooled portion of the condenser and the condenser output. State point [6] was the isenthalpic expansion valve output and the evaporator input. Finally, state point [7] was the point within the

evaporator when the working fluid became a saturated vapor before entering the superheated region and beginning again at state point [1].

The first two temperature relationships involved the differences in the determined ambient and space temperatures and the working fluids in the condenser and evaporators respectively. The next two temperature relationships determined the amount of superheating and subcooling to be done in the system. The following equations represent the relationships of the temperatures in the system.

$$T[4] = T_{amb} + \Delta T_{sat} \tag{10}$$

$$T[6] = T_{space} - \Delta T_{evap,in} \tag{11}$$

$$T[1] = T[7] + T_{superheat} \tag{12}$$

$$T[5] = T[4] - T_{subcooling} \tag{13}$$

T[4] and T[6] were based solely off of the given temperature difference of the working fluid and the given set temperatures. T[1] and T[5] were based off the temperatures and T[7] and T[4], the edges of the two-phase region and determined how much superheating and subcooling, respectively, were to be done.

The next important parameters to be determined were the qualities of the state points at the edges of the two-phase region. The qualities of state points [3], [4] and [7] could be assumed due to them being saturated liquids or vapors. State point [4]

was a saturated liquid so it could be determined that it had a quality of 0. State points [3] and [7] were saturated vapors so they could be assumed to have qualities of 1.

Each state point requires two independent parameters in order to determine the remaining parameters. Anywhere within the two-phase region, pressure and temperature are not independent parameters. Therefore, two more relationships must be made in order to complete the system analysis. First, it can be assumed that the expansion process is isenthalpic. This means that there is no change in enthalpy between state points [5] and [6]. Therefore, it can be assumed that

$$h[5] = h[6] \tag{14}$$

The final important relationship used to analyze the cycle was the relationship of the enthalpies over the compression process, or between state points [1] and [2]. The compression process is not isentropic so there is some entropy loss over the compressor. Therefore, entropy of state point [1] does not equal to the entropy of state point [2]. In order to relate the entropies, the isentropic efficiency must be used. First, state point [2s] must be determined which makes the assumption that the compression process is isentropic. Pressure of state points [2] and [2s] are the same as well. Assuming the compression process is isentropic; it can be assumed that,

$$s[1] = s[2s] \tag{15}$$

Now, using the pressure and entropy at state point [2s], the enthalpy, h[2s] can be determined. Finally, the enthalpy at state point [2] can be determined using the isentropic efficiency relationship shown in the following equation.

$$\eta_{\text{isen}} = \frac{h[2s]-h[1]}{h[2]-h[1]} \tag{16}$$

Now, with the enthalpy and pressure at state point [2], the remaining parameters can be determined. Using all of the relationships stated previously, the equations can be simultaneously solved through EES to determine the parameters at each state point. The remaining parameters not originally determined in the initial evaluation can be determined using the two independent existing parameters at each state point.

Once all of the system parameters were determined, the cooling capacity, power inputs and COP could be determined. First, the mass flow rate of the working fluid was calculated using the volumetric efficiency relationship.

$$\eta_{\text{vol}} = \frac{\dot{m}}{\rho_{comp,in} * V_{disp} * \left(\frac{RPM}{60}\right)} \tag{17}$$

The ideal compressor power could then be determined by the equation,

$$\dot{W}_{comp,ideal} = \dot{m} * (h[2s] - h[1]) \tag{18}$$

This would be the power input of the compressor if it were a isentropic compression, but due to the compressor efficiency less than unity calculated by the

equation in Table 1, this was only the ideal compressor input power used to determine the actual compressor input power required.

$$\eta_{\text{comp}} = \frac{\dot{W}_{comp,ideal}}{\dot{W}_{comp,real}} \tag{19}$$

The actual compressor power input was determined using the isentropic efficiency equation. Next, the heat transferred in the two heat exchangers was determined.

$$\dot{Q}_{evap} = \dot{m} * (h[1] - h[6]) - \dot{W}_{fan,evap} \tag{20}$$

$$\dot{Q}_{cond} = \dot{m} * (h[2] - h[5]) \tag{21}$$

The power of the evaporator fan was added into the evaporator heat transfer because the fan motor in the evaporator also acted as a heat load. The power input of the evaporator fan will be determined at a later point in the analysis. The heat removed from the condenser was determined assuming there were no external heat loads.

The total power input required to power the system can be determined by summing the power input of the compressor, evaporator fan motor and condenser fan motor. The required fan motor powers were assumed based on fan motors used in preexisting units. For now, the power of the fan motors mainly affects the COP which can be adjusted later.

$$\dot{W}_{Total} = \dot{W}_{comp,real} + \dot{W}_{fan,evap} + \dot{W}_{fan,cond} \quad (22)$$

The cooling capacity of the air conditioning unit is represented by the heat transferred to the evaporator. Therefore, the COP of the system can be determined by dividing the cooling capacity by the total power input.

$$COP = \frac{\dot{Q}_{evap}}{\dot{W}_{Total}} \quad (23)$$

In this model, the evaporator load, or the cooling capacity was set based on the previous AHU model. Changing the cooling capacity in this model will change the compressor displacement. Once the standard VCC was modeled, the $\Delta T_{evap,in}$ value was adjusted to a temperature above the dew point temperature of the air. By increasing the evaporator inlet temperature to above the dew point temperature of air at these conditions, it will ensure that all cooling done will be solely sensible cooling. No moisture will be removed from the air at these conditions. By keeping the cooling capacity constant but adjusting the evaporator inlet temperature, the pressure ratio will decrease and the compressor power consumption will then decrease. This is where the potential energy savings of this system occur.

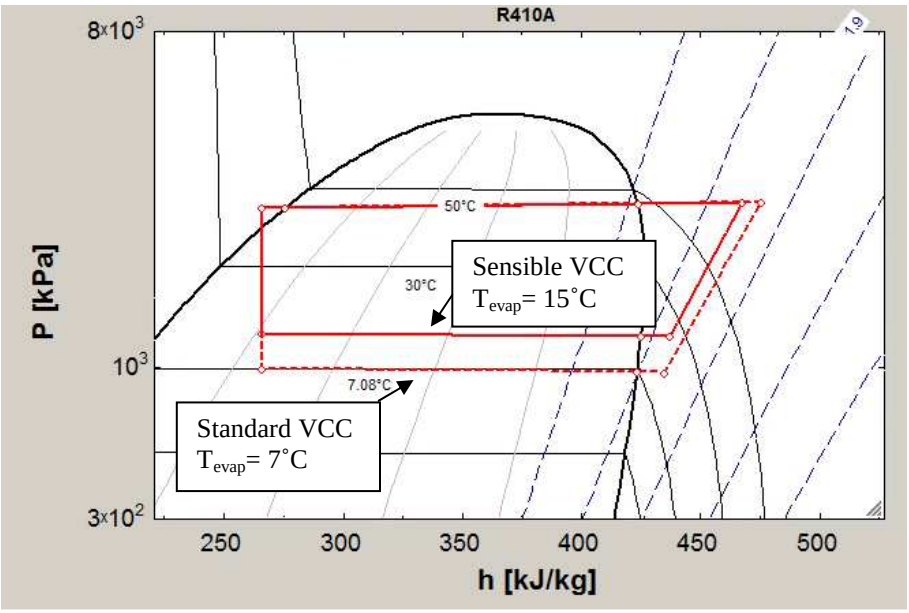

Figure 8: Comparison of Standard and Sensible Only VCC

Figure 8 shows P-h diagrams of two VCC's. The dotted line represents a standard VCC for a 2.93 kW cooling capacity. The solid line represents a VCC for a 2.93 kW cooling capacity, but with 100% sensible cooling. Just from looking at the plot it is obvious that the pressure ratio of the sensible only VCC is lower and less work needs to be done in the compressor.

Table 4: Comparison of Modeling Results for Two VCCs

Parameter	Unit	Standard VCC	Sensible Only VCC
Q_{evap}	kW	2.93	2.93
Pressure Ratio	-	2.9	2.2
W_{comp}	kW	0.773	0.559
V_{disp}	cm^3/rev	10.09	7.58
COP	-	3.12	4.05
$T_{evap,in}$	°C	7	15

The values in Table 4 are subject to change such as the COP or compressor power based on fan power requirements and compressor efficiencies, but the model at least shows the significant change due to the shift to only sensible cooling. The latent

load is removed by the DW which is powered by a 12W motor so the additional energy consumption is negligible to make the unit a 3.5 kW unit. The COP will still remain close to 4 due to an increase in fan power consumption which will be addressed later in the design process. Now with the additional modeling results for the evaporator and condensers, a more in depth modeling of the heat exchangers can be done.

2.2: Heat Exchanger Model

The first step in modeling the heat exchangers was modeling the preexisting heat exchangers used in the original PTAC unit. From there, designs that meet the requirements of the new unit could be made based off the preexisting design. This was done for the evaporator and the condenser. The condenser in the preexisting unit becomes two separate condensers for the desuperheat region and the remaining heat transfer from the refrigerant.

2.2.1: Evaporator

The preexisting heat exchangers were tube-and-fin type heat exchangers. The parameters of the evaporator was measured and used in CoilDesigner [3] to model the preexisting coil.

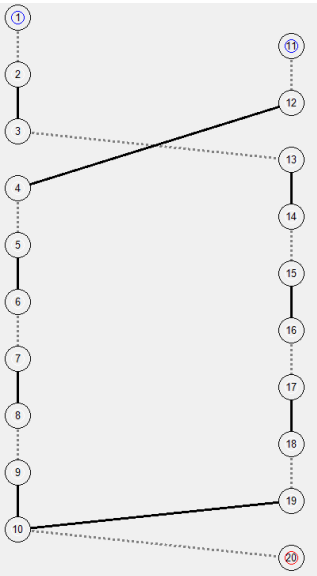

Figure 9: Preexisting Evaporator Coil

The coil was a staggered convergent two bank, ten tubes per bank design. Due to the profile of the PTAC unit, the preexisting evaporator was wide and short. This allowed for a significantly large air flow area, allowing for a lower air flow velocity.

The new evaporator was designed to be a microchannel heat exchanger (MCHX). The MCHX can be significantly smaller than the tube-and-fin heat exchanger which was necessary in order to add the DW to the system. A smaller surface area means a larger air flow velocity and a larger air flow pressure drop, but the pressure drop would be more negligible in comparison to the pressure drop over the DW.

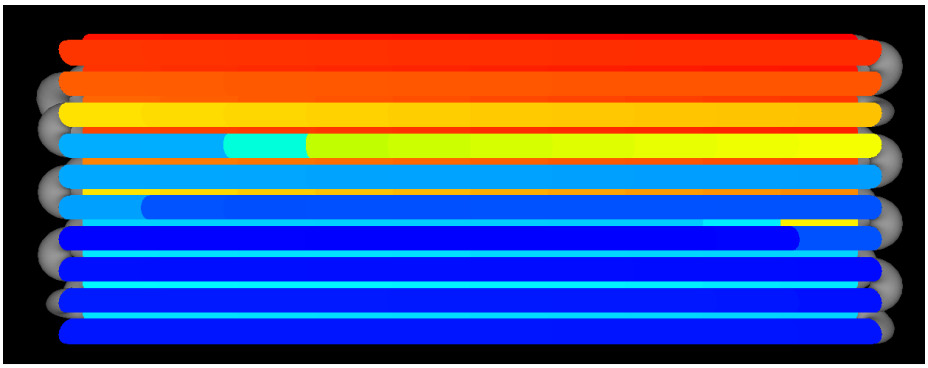

Figure 10: Preexisting Evaporator Tube-and-fin Coil

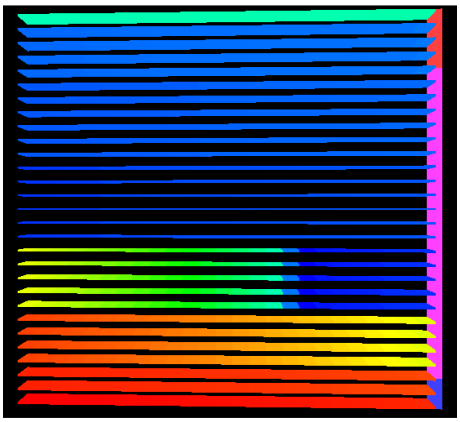

Figure 11: SSLC PTAC MCHX Evaporator

Figure 10 and Figure 11 show the design of the original evaporator and the MCHX designed for the SSLC PTAC unit.

Table 5: Evaporator Coil Comparison

Parameter	Unit	Preexisting Evaporator	SSLC MCHX Evaporator
Length	m	0.66	0.29
Height	m	0.254	0.281
Cooling Capacity	kW	3.8	3.3
Air Flow Rate	m^3/h	680	934
Air Pressure Drop	Pa	27	54
Refrigerant Pressure Drop	kPa	31.4	346
Tube Material Mass	kg	3.35	0.29

There are a few negative effects of using a MCHX over a tube-and-fin heat exchanger, but in the case of the SSLC PTAC unit, the good outweighs the bad. The profile is smaller so the air pressure drop is doubled in the MCHX. This issue is less negligible in the combined system due to the large pressure drop that needs to be overcome through the DW. A larger and more power consuming fan is already necessary in the SSLC unit. There is a higher refrigerant pressure drop as well which will reduce the increased COP of the system.

The positives of the MCHX are what make it a better choice for the SSLC unit. Due to the more complicated air flow paths required in the unit, the smaller heat exchanger will be extremely beneficial. Also, the lower amount of material will reduce the cost of the heat exchangers. The DW will add a large additional cost to the overall system so replacing preexisting parts with less expensive components is extremely beneficial.

2.2.2: Desuperheat Condenser and Condenser II

Similarly to the evaporator, the preexisting condenser was modeled before designing a new heat exchanger. The difference from the original condenser though is that the single larger tube-and-fin condenser is being replaced by two smaller heat exchangers. The condenser on the preexisting PTAC unit was taller and narrower than the evaporator because air intake for cooling the condenser was done from the sides. The condenser also had two banks, but instead had 22 tubes per bank.

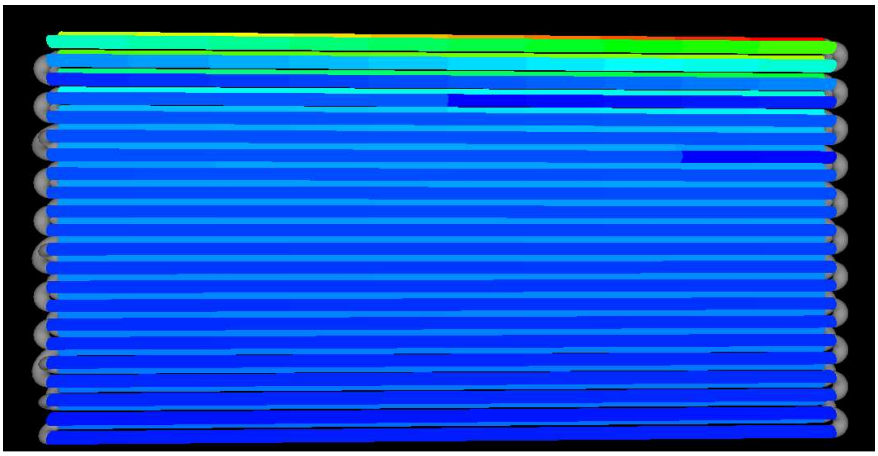

Figure 12: Preexisting PTAC Unit Condenser Coil

Figure 12 shows the coil design of the preexisting condenser. The new desuperheat condenser was designed as a MCHX of the same dimensions as the evaporator. In order to reutilize the waste heat removed from the desuperheat condenser, the air needed to reach a temperature of 50°C. In order to remove heat from only the hottest region, the desuperheat condenser only condenses the refrigerant until it reaches the transition point to the two-phase region. The MCHX needed to be designed to only operate in that region. Also, in order to heat the air so high, the air flow rate needed to be low, which is why the same sized MCHX is used for a 1 kW condenser and the 3.2 kW evaporator.

The condenser II exhausts the remaining heat into the environment. The MCHX used for condenser II is larger than the first two heat exchangers. This allows for lower fan power consumption and a larger heat transfer.

Table 6: Condenser Coil Comparison

Parameter	Unit	Preexisting Condenser	SSLC MCHX Desuperheat Condenser	SSLC MCHX Condenser II
Length	m	0.67	0.29	0.34
Height	m	0.35	0.281	0.33
Heat Capacity	kW	4.01	0.9	2.7
Air Flow Rate	m^3/h	1,274	177	1,274
Air Pressure Drop	Pa	0.46	7	52
Refrigerant Pressure Drop	kPa	139	106	114
Tube Material Mass	kg	1.55	0.29	0.4
Air Outlet Temp	°C	45	51	37

Similarly to the evaporator, there is a higher refrigerant pressure drop and air side pressure drop. The smaller size of the condensers is even more beneficial than the reduction in size of the evaporator though. Both condensers need to be placed on the backside of the PTAC unit with a common outlet so space is limited. Because the desuperheat condenser operates immediately after the compressor in the superheat region, the air temperature can reach 50°C with a low flow rate of approximately 180 m^3/h. The tube material mass is also lower for both condenser combined which again is beneficial to the overall cost of the system.

2.3: Cycle Model

After the coils were individually designed, the entire system could be modeled and optimized using VapCyc [5]. VapCyc is a program that can incorporate heat exchangers designed in CoilDesigner into an entire vapor compression cycle designed at the user's discretion. VapCyc gives the engineer the freedom to layout the components in any manner. First, the original PTAC unit components were

implemented into VapCyc to validate the model. Then, the coils were replaced by the new MCHX's to model the SSLC unit.

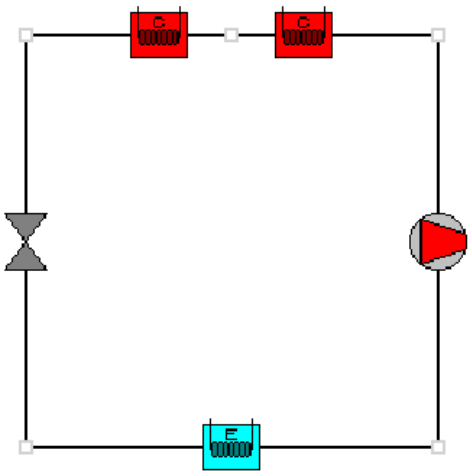

Figure 13: SSLC System Diagram in VapCyc

Both systems were run using VapCyc. The superheat, subcooling, expansion valve parameters and compressor parameters were all set equally in both setups.

Overall System Results

System Energy Balance	0.569	W		System State Points	Temperature	Pressure
				Junction	T [K]	P [Pa]
System COP	6.215			1	296.171	1184988.386
System EER	21.207	Btu/W-hr		2	341.695	2538172.658
				3	307.867	2403044.418
Total Refrigerant-side Capacity	3122.97	W		4	288.451	1268645.395
Net Air-side Capacity	3122.97	W		5	313.138	2418598.90
Power Consumption	502.479	W				

Figure 14: VapCyc Results for SSLC Unit

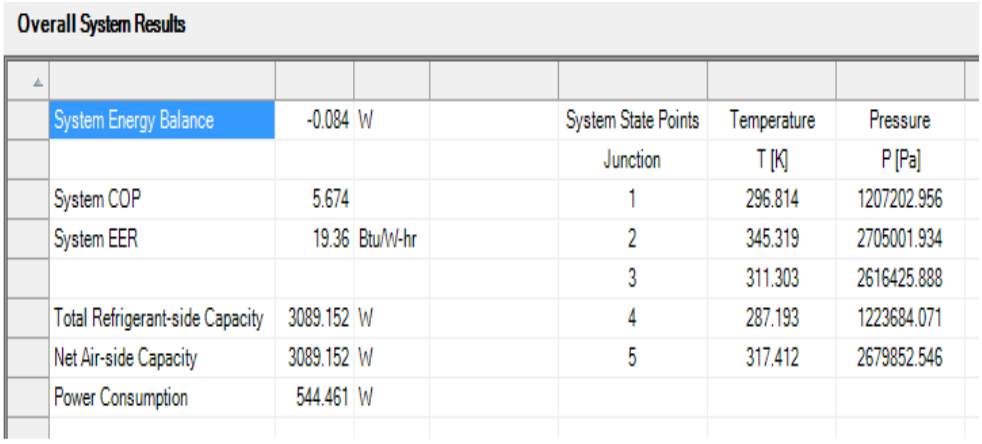

Overall System Results

System Energy Balance	-0.084	W	System State Points	Temperature	Pressure
			Junction	T [K]	P [Pa]
System COP	5.674		1	296.814	1207202.956
System EER	19.36	Btu/W-hr	2	345.319	2705001.934
			3	311.303	2616425.888
Total Refrigerant-side Capacity	3089.152	W	4	287.193	1223684.071
Net Air-side Capacity	3089.152	W	5	317.412	2679852.546
Power Consumption	544.461	W			

Figure 15: VapCyc Results for Preexisting PTAC Unit

Figure 14 and Figure 15 show the VapCyc results for both cases. Using the SSLC heat exchangers and reducing the compressor displacement increased the COP of the VCC. This increase in COP is not counting the additional cooling capacity due to latent cooling from the DW with negligible additional power consumption. It is important to note though that the COP shown in the VapCyc results does not reflect the actual COP of the system because they do not account for fan power input which would bring the COP down to a more reasonable 3.5-4.0 range. The VapCyc model only shows the effect of the newly designed VCC. It is also important to point out that the 50°C air outlet for the desuperheat condenser is also achieved when running the entire system, not just for the stand alone CoilDesigner model which is important to the success of the SSLC system.

Chapter 3: Prototype Design

Once the heat exchangers were modeled, designed and properly sized, the design layout could begin to take shape. The original prototype was used as a starting point, but the design had to be changed in order to create a unit that was more practical for manufacturing purposes. The other components needed to be sized as well. The main components that needed to be sized were the DW and the three fans; one for each of the heat exchangers.

3.1: Prototype I Design versus Prototype II Design

The first prototype of the DW assisted SSLC unit was successful in reaching a 30% increase in energy efficiency, but that loses its engineering significance if the unit is not affordable or inconveniently designed.

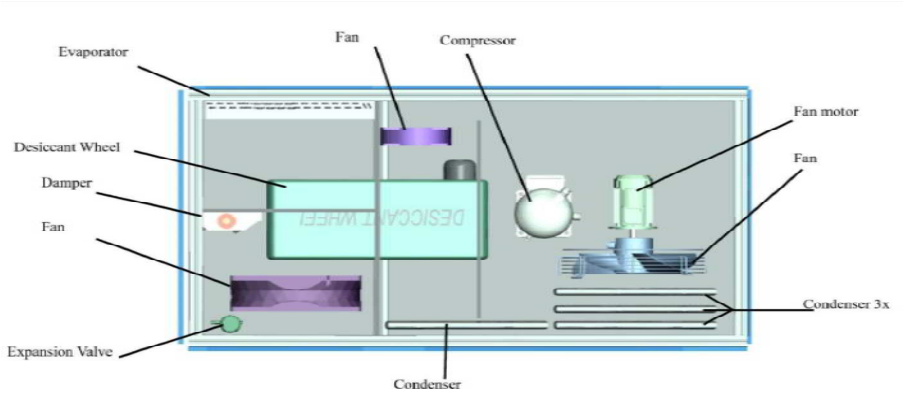

Figure 16: SSLC Prototype I Layout [2]

Figure 16 shows the layout of the first SSLC prototype. There are two big issues with the first prototype that were addressed in the second prototype. First is the size of the unit.

Table 7: SSLC Dimensional Comparison

Parameter	Height [m]	Width [m]	Depth [m]	Volume [m^3]
Amana 12,000 BTU	0.41	1.07	0.56	0.80
Prototype I	0.64	1.20	0.60	1.51
Prototype II	0.41	1.07	0.67	0.95
Δprototype	-0.23	-0.13	0.07	-0.56

Originally the goal was to design a window sized AC unit with the SSLC technology, but due to the required air flow paths and additional components such as the DW it was impossible. The next larger sized unit was the PTAC unit, which was similar in size to the first prototype. The dimensional restrictions were set for the second prototype so that an old PTAC unit could be retrofitted with a new SSLC PTAC unit without additional construction or alterations to the building. Table 7 shows the required changes to the original prototype that need to be made to meet the requirements in the second prototype. In order to make up for space in the length and width dimensions, the depth of the unit is larger than the standard unit, but that would not affect the unit's ability to retrofit an old PTAC unit.

The second big issue in the first prototype can be seen in Figure 16. The process air loop's inlet is on the front of the unit and the outlet is on the back of the unit. The exhaust loop's inlet is on the back of the unit and the outlet is on the front of the unit. In the PTAC unit, the mass transfer can only flow through the front and back of the unit, but the process air's inlet and outlet must only flow through the front and the exhaust must only flow through the back. This makes for a more complicated air flow path due to the DW because both loops must flow through the DW. Therefore, in the second prototype, the DW needs to be turned 90 degrees and both air loops need to make sharp 180 degree turns. This increases the pressure drop,

increasing the required size of all fans. The first prototype also incorporated a radiative heat exchanger wall as an additional evaporator, so in the second prototype, the single MCHX evaporator must also have a higher cooling capacity. Because the second prototype is smaller and requires more compact air flow loops, the footprints of the fans also need to be smaller to meet the overall size restrictions.

3.2: Desiccant Wheel Sizing

The size of the DW is important for two reasons. The first reason is that the size of the wheel determines the capacity of the wheel based on the amount of desiccant material. The latent capacity and moisture removal rate calculated in the latent cooling load were used to determine the size of the DW. The latent capacity and moisture removal rate of the system are 0.92 kW and 0.365 g/s, respectively. The second important factor when deciding the size of the DW is the height restriction of the unit. The maximum height of the unit is 410 mm, but after subtracting the height of the casing, the space for components is reduced to 381 mm. The size of the casing around the DW also needs to be taken into account. The casing requires about 38.1 mm on all sides of the wheel, making the maximum size of the wheel to be 304.8 mm. Based on information from the manufacturer, the wheel was sized at a diameter of 300 mm (~12 in) and 90 mm (~3.5 in) thickness. The 90 mm thickness oversized the capacity of the wheel by about 20% for testing purposes. The DW is the largest component in the SSLC unit and the entire layout is designed around the wheel.

3.3: Fan Sizing

Each of the heat exchangers requires its own fan. Because there is an additional condenser in the SSLC unit, a third fan needed to be incorporated into the design. A single air flow loop cannot be used for both condensers due to the low air flow rate required to maintain the higher regeneration temperature. However, a higher air flow rate is required on the condenser II in order to exhaust the remaining heat from the system. Additionally, the dimensions of the fan as well at the power consumption needed to be taken into account when choosing fans. Because of the high pressure drop associated with the DW as well as the tight and complicated air flow paths, more powerful fans were required for the evaporator and the desuperheat condenser. Overall, the fan power consumption will be higher than preexisting PTAC units, but still significantly less than the amount of power saved by downsizing the compressor.

All fans chosen for experimental and testing purposes were chosen to be variable speed fans. They were also oversized by 20% from the expected pressure drop. After testing and experimentation is completed, more specifically sized fans can be chosen, optimizing the system as well as reducing the cost of the fans and the overall unit.

3.3.1: Evaporator Fan

Based on the manufacturer's data, the pressure drop through the DW was calculated to be roughly 170 Pa. In addition to the DW, a significant pressure drop was also assumed based on the air flow path. Not only is the air flow path restrictive,

the path also requires the air to turn 180 degrees. The required pressure drop was estimated at a minimum of 300 Pa.

Not only did the fan need to be powerful enough to overcome a high pressure drop, it also needed to produce a high air flow rate. The standard PTAC unit uses a cross flow fan which does not have the pressure drop due to turning the air 180 degrees. The cross flow fan does not have the required power to overcome the required pressure drop. A motorized impeller fan was chosen for the evaporator fan due to its high pressure lift and air flow rate.

Figure 17: Motorized Impeller Fan [9]

The additional purpose of using the motorized impeller fan is to avoid directly forcing the air to turn 180 degrees, similar to the cross flow fan. Figure 17 shows the motorized impeller fan used for the evaporator. The motorized impeller fan's inlet is vertical whereas the outlet is horizontal. The fan is capable of turning the air 90 degrees, reducing the pressure drop due to the sharp turns.

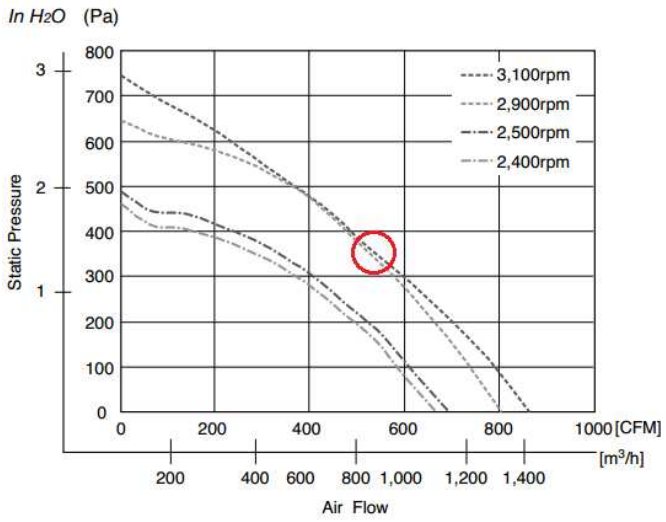

Figure 18: Evaporator Fan Performance Curve [9]

Figure 18 shows the performance curve of the motorized impeller fan. At the design point of 934 m^3/h, the fan has a pressure lift of 350 Pa. In order to benefit from the SSLC technology, the fan power cannot be significantly greater than a standard unit's fan power and cancel out the compressor power reduction. The chosen fan has a rated power consumption of 145 W at maximum power [9]. The fan is not expected to run at maximum power, so the power consumption will be even less than 145 W. The evaporator fan will require the highest power consumption and the estimated less than 145 W is right around what is to be expected. An inlet nozzle ring was also used in order to aid the air flow through the inlet maximizing the potential of the fan.

3.3.2: Desuperheat Condenser Fan

The desuperheat condenser fan must also overcome the pressure drop of the DW, as well as the desuperheat condenser. The pressure lift required was estimated

to be 250 Pa. The required air flow rate was only 177 m^3/h in order for the air to reach the required regeneration temperature of 50°C.

Figure 19: Desuperheat Motorized Impeller Fan [10]

The desuperheat fan was chosen to be a centrifugal fan with a prebuilt case around the impeller to direct the air flow in a single direction. Figure 19 shows the fan used for the desuperheat condenser. Similarly to the evaporator fan, the centrifugal fan is used to turn the air 90 degrees without the associated pressure drop of a 90 degree turn. The additional positive aspect associated with the centrifugal fan is the built in inlet nozzle in the casing as well as the easily controlled inlet. Unlike an axial fan, the inlet can be sealed to create a separate air flow path directly vented out of the DW and into the inlet of the fan.

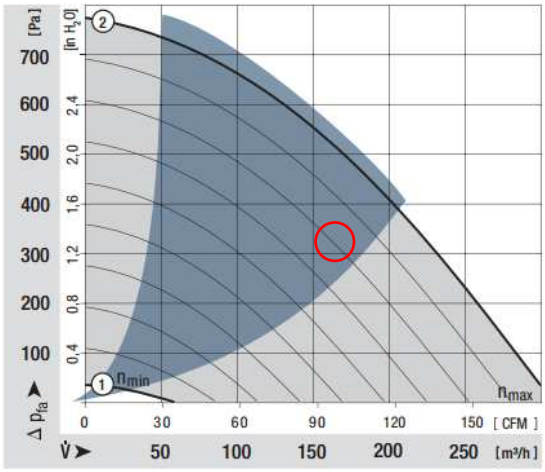

Figure 20: Desuperheat Fan Performance Curve [10]

Figure 20 shows the performance curve of the specified centrifugal fan. At 177 m^3/h, the pressure lift is 325 Pa, significantly more than the estimated pressure drop. The over sizing allows for a buffer in case the pressure drop is larger than estimated. The maximum power output of the fan is 64 W [10]. At the specified design point, the output power is estimated to be closer to 48 W. The desuperheat fan should be the lowest power consuming fan of the three. 48 W was decided to be sufficient and not have an adverse effect on the overall COP.

3.3.3: Condenser II Fan

The condenser II fan was originally chosen to be the axial fan used in the standard PTAC unit. Once the design and construction began, the large footprint of the axial fan with the extruding motor could not fit within the design constraints. The objective when choosing a new condenser fan was to find a fan with minimal additional power consumption, with similar air flow rate and a smaller footprint. In order for a smaller fan to produce the same flow rate as a larger fan, the RPM must be higher, therefore increasing the power consumption. Unlike the first two fans, this air

flow path did not flow through the DW. Also, the surface area of the condenser II was larger than the desuperheat condenser and evaporator. Therefore, pressure drop was less of an issue with this fan. Based on the original PTAC unit's exhaust airflow path, the required pressure drop to overcome was roughly 40-50 Pa. The original PTAC unit's exhaust airflow path did an immediate 180 degree turn with a 40 W axial fan.

Figure 21: Condenser II Axial Fan [11]

Figure 21 shows the axial fan chosen for the condenser. The motor is contained within the profile of the blade, and the blade is flatter than the original condenser fan. The depth of the fan was reduced from about 203 mm to 76 mm. The diameter of the fan is 280 mm, well within the height restriction of the unit. The reduced depth provides more freedom in the placement of the fan as well as the condenser in the design.

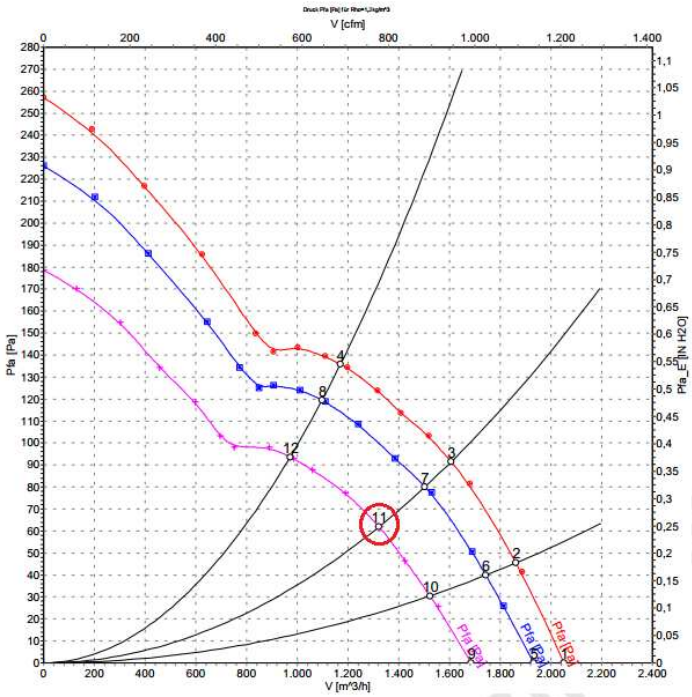

Figure 22: Condenser II Fan Performance Curve [11]

Figure 22 shows the performance curve of the axial fan chosen for the condenser. The design point of 1,274 m^3/h has a pressure lift of 60 Pa, more than the estimated requirement of the fan. At this point, the power consumption of the fan is 78 W. The power consumption of this condenser fan was less than the fan used for the condenser in the original prototype, assuring that the additional power consumption over the original fan will not impact the 30% efficiency increase objective. The condenser may not require that high of a flow rate as well, reducing the power consumption even more.

3.4: Layout Design

Layout design was done using CAD software Solidworks [12]. The purpose of the CAD design was to layout the large components of the system optimally. Many iterations of the CAD drawing were done until the final design was chosen. Each component was modeled or represented by a component of the same dimensions. The CAD drawing was also used to layout the airflow paths, and to determine whether there would be sufficient space for inlets, outlets, bypasses and air flow.

Once the main unit was modeled and constructed, the process side air duct was designed in CAD. The process side air duct represents the space requiring cooling within the environmental chamber. The process side air duct was also required to include all required instrumentation as well as a humidifier and heater to rehumidify and reheat the air to inlet conditions.

3.4.1: PTAC Unit Layout

As stated previously, the PTAC unit size was set based on the preexisting PTAC units. The overall length and height for the components to fit within were 1016 mm and 381 mm, respectively. There was more freedom in the depth of the unit so it was set at 622 mm.

The largest component in the unit was the DW, therefore the design layout was modified accordingly.. The DW also required a casing and a motor, making it larger than the diameter of the DW material.

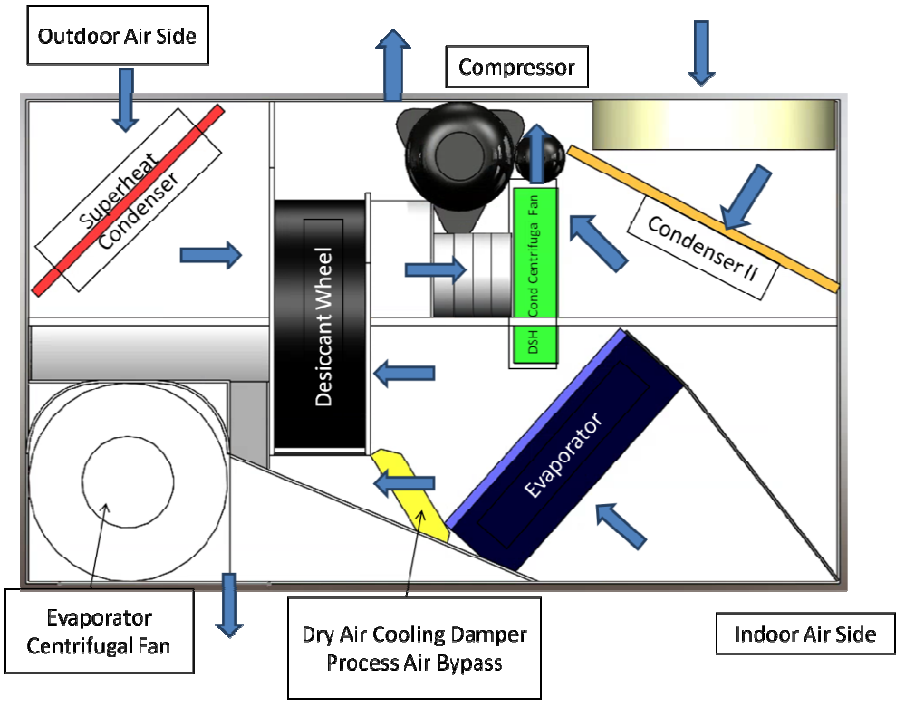

Figure 23: PTAC Layout Design in SolidWorks

Figure 23 shows the initial layout of the PTAC unit. The blue arrows show the air flow path through evaporator and condenser side. The indoor air side first flows through the evaporator, then is split between the DW and the damper in a ratio dependent on the necessary dehumidification, and then is drawn into the evaporator fan.

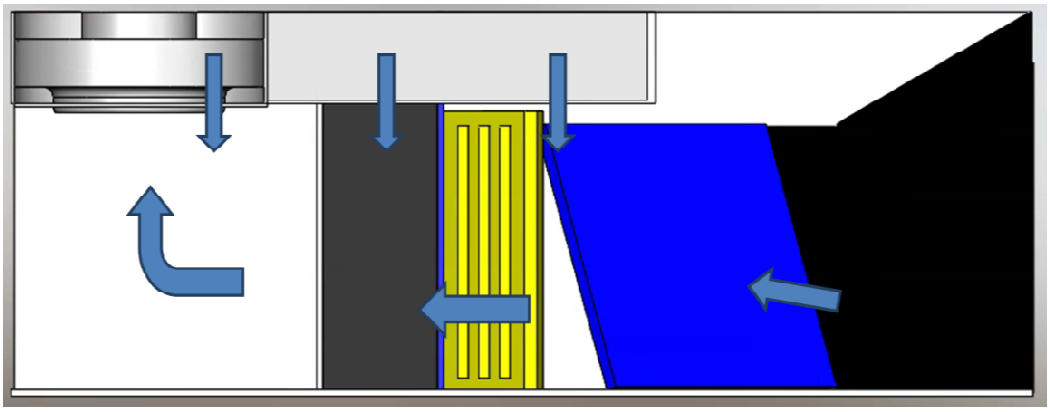

Figure 24: Evaporator Air Loop PTAC Front View

Figure 24 shows the indoor air side loop from the front view. As mentioned previously, the centrifugal evaporator fan assists the air flow and reduces the pressure drop associated with sharp right angle turns. The evaporator is installed with an angle in order to reduce the sharp turns as well. The closer to parallel the evaporator is to the DW and bypass opening, the less significant the pressure drop due to duct geometry. The evaporator cannot sit exactly parallel to them though due to space constraints.

The outlet was designed to be consistent with the outlet of preexisting PTAC units. The wider outlet allows for a better distribution of air throughout the space. Additional ducting needed to be added to the fan in order to create the necessary outlet.

The damper can be opened to certain percentages depending on the required dehumidification. In a case where no dehumidification is necessary, the bypass can be fully opened, reducing the power consumption of the fan.

The desuperheat condenser was also angled to be closer to parallel with the DW as seen in Figure 23. The desuperheat loop also was designed with a bypass for a no dehumidification or “dry cooling” case. Since the fan is set after the DW and draws the air through the loop, the bypass needed to be ducted directly back into the same duct after the DW.

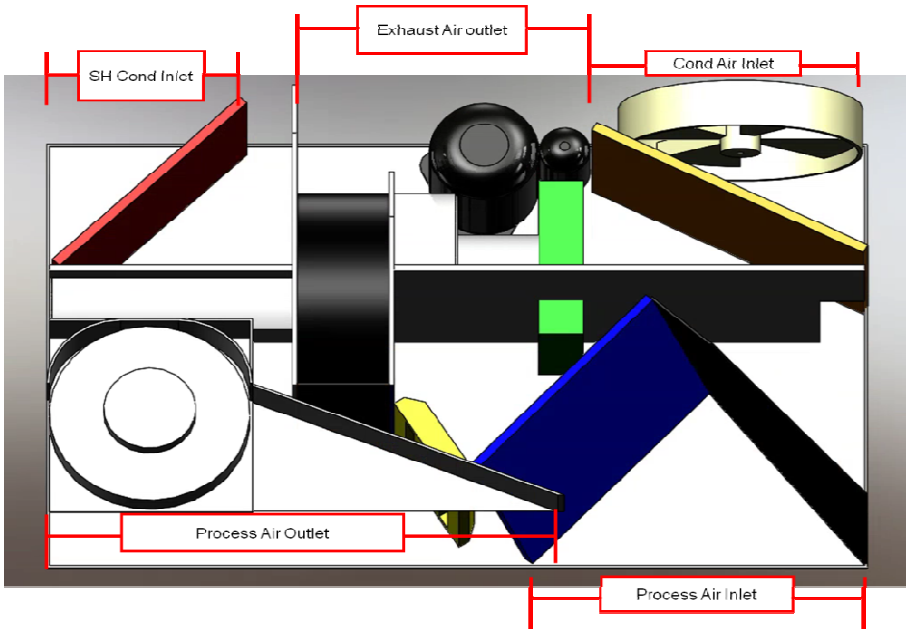

Figure 25: Inlet/Outlet Diagram

The desuperheat condenser and condenser II share a common outlet as shown in Figure 25. At the outlet, all of the air is exhaust air so the mixing does not matter. Both exhaust outlets also flow directly over the compressor. Cooling the compressor increases the performance of the compressor. This design strategy implemented in standard AC units.

The DW was also turned 90 degrees from its original position in the first prototype. It was not practical to leave it the way it originally was due to the process and exhaust loops being separated down the middle of the unit. The idea of splitting the DW top and bottom was also considered, but due to the size of the heat exchangers, this was also impractical.

This design layout was the most practical and remained close to the original PTAC unit design. It allowed for the mass transfer requirements to be met (only across the front and back faces) and fit all of the components in the most practical

way. This design also allowed for bypasses which could increase the efficiency even more in certain operating conditions.

3.4.2: Process Air Side Duct Design

The process air side duct needed to create a closed loop for the process air. The entire apparatus was set up within an environmental chamber which would simulate the ambient conditions. The process air side loop would simulate the conditioned space. The process air side duct also needed to accommodate all necessary instrumentation as well as an electric heat and humidifier. The heat and humidifier would reheat and humidify the air back to the required inlet conditions after the air was processed, cooled and dehumidified.

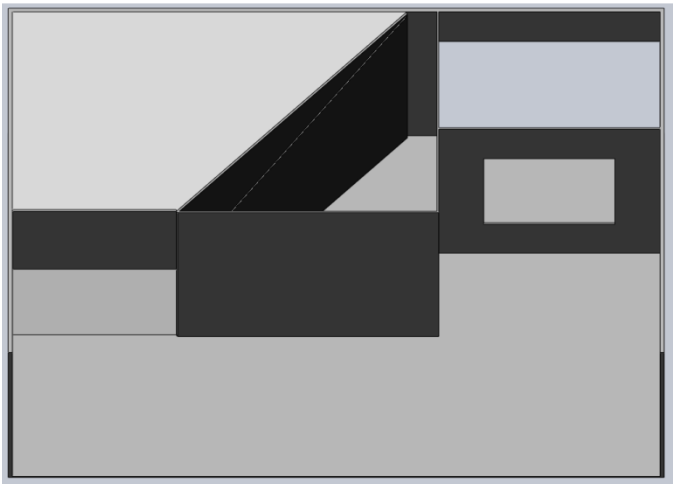

Figure 26: Process Air Side Duct Model: Angled Top View

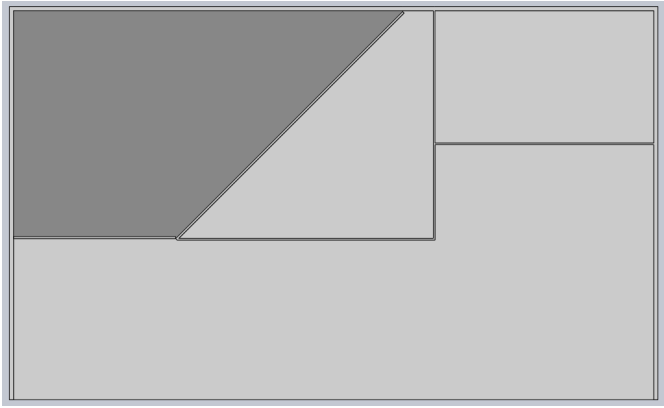

Figure 27: Process Air Side Duct Model: Top Down View

Figure 26 and Figure 27 show the angled top and top down view of the process air side duct, respectively. The process air side duct attaches to the front of the PTAC unit and lines up with the process side inlet and outlet. The inlet of the air duct (outlet of the PTAC unit) channels the air into a square duct. The square duct has sufficient room to mount the humidifier and heater, as well as another fan. The fan in the process duct is used to balance to the pressure drop across the duct. The sharp turns are not as important in the duct because a fan can be used to balance the pressure, and the power consumption of the fan does not affect the overall COP of the system. This part of the design was for experimental purposes only.

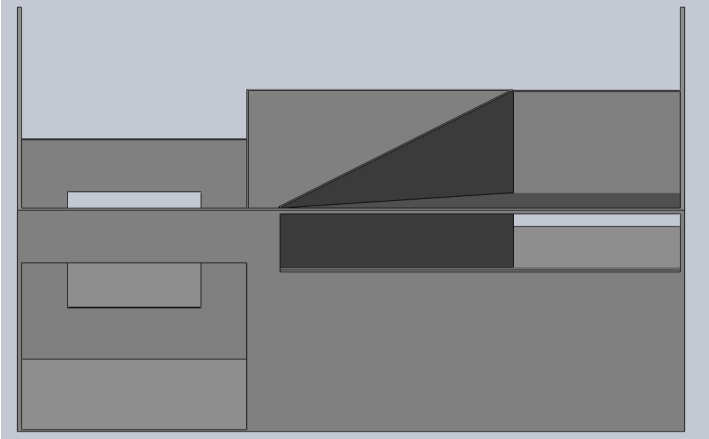

Figure 28: Process Air Side Duct Model Back View

Figure 28 shows the back side of the process air side duct where it connects to the PTAC unit. The long and thin inlet to the duct can be seen being channeled into a square shape duct to create a uniform shaped duct back to the outlet of the process air side duct. Additionally, a partition with a square hole was added in the design to accommodate an air mixer. The mixer blends the air after it is heated and humidified to ensure there are no uneven high temperature points in the flow. The mixers require a specified upstream and downstream length to ensure proper mixing which were taken into account when designing the entire duct.

3.4: Process Diagram

The process diagram was created based on the CAD modeling done and was adjusted during the construction of the experimental test setup.

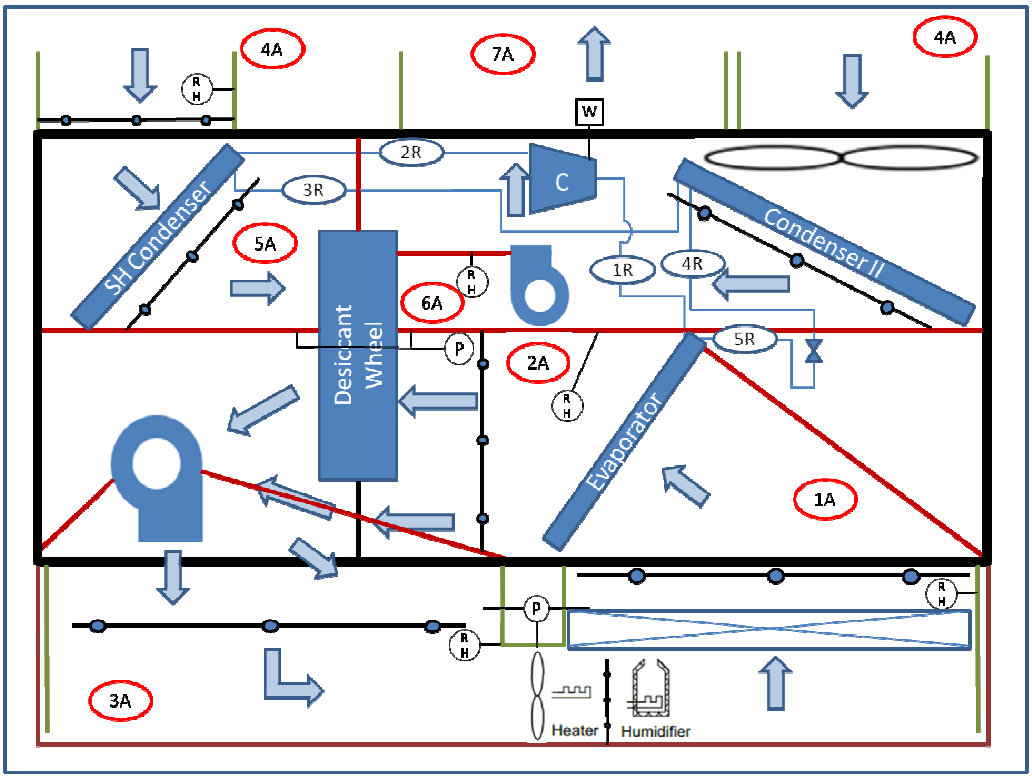

Figure 29 SSLC PTAC Unit Process Diagram

Figure 29 shows the complete process diagram of the SSLC PTAC unit. The diagram consists of the two air loops as well as the refrigeration loop. The diagram also shows the placement of instrumentation within the system.

The first air side loop is the process air side loop. State point 1A is the space air inlet. The air passes through the evaporator to state point 2A, reducing the temperature of the air. Then, the cooled air flows through the DW where the moisture is removed, coming out at state point 3A cool and dry at the designated temperature and humidity ratio. Finally, the air is reheated and rehumidified back to the inlet condition at state point 1A.

The next air side loop is the exhaust airside loop. The air on this side comes in from the environment at state point 4A. The air flows over the desuperheat

condenser and is heated to 50°C at state point 5A. Next, the air flows through the DW, regenerating the desiccant material. Regeneration of the material means that the hot air removes the moisture from the desiccant material so the wheel can spin and dehumidify the process air again. After going through the wheel, the air drops a few degrees below 50°C but has a higher humidity. Finally, the hot and humid air is exhausted through the centrifugal fan to the common exhaust outlet at state point 7A.

In addition to the desuperheat half of the exhaust loop, there is also the air cooling the direct condenser. The air comes in at ambient temperature at state point 4A, flows over the condenser removing the heat from the refrigerant and is exhausted to state point 7A, the common exhaust outlet.

The final loop in the process diagram is the refrigeration loop. State point 1R is the evaporator outlet and compressor suction. At this point, the refrigerant should be a low temperature, low pressure vapor. State point 2R is the compressor discharge and desuperheat condenser inlet. After going through the compressor, the refrigerant becomes a high temperature, high pressure vapor. State point 3R is the desuperheat condenser outlet and condenser II inlet. This is the point at which the refrigerant is crossing from the superheat vapor region to the two-phase region. In a standard vapor compression system, this point takes place within a single condenser, but in the case of the SSLC unit, the second condenser is necessary for waste heat utilization. State point 4R is the condenser outlet and expansion valve inlet. After leaving the condenser, the refrigerant should still be in the two-phase region at a high temperature, but a lower temperature. State point 5R is the isenthalpic expansion valve outlet and evaporator inlet. When the refrigerant passes through the expansion

valve, the temperature and pressure drop significantly. Finally, the refrigerant flows through the evaporator and comes out at a higher temperature due to heat exchange from the process air flow.

Figure 29 shows three different types of instrumentation used on the air flow side; temperature grids, differential pressure transducers and relative humidity sensors. The temperature grids were placed at all necessary point where it was important to know the temperature of the air. The entire process air side is important, in order to determine the cooling capacity of the system. Immediately after the desuperheat condenser is also important to ensure the air is reaching the required regeneration temperature. It is also important to know the air temperature after the condenser to ensure enough heat is being expelled from the system. Monitoring the temperature can also make the system more efficient by making sure not to run the exhaust fan higher than it needs to be for the specified cooling capacity.

The differential pressure transducers have two different roles. The differential pressure transducer over the DW can accurately determine the pressure drop over the DW for later optimization of the system. The second differential pressure transducer is used to equalize the pressure through the process air side duct. It can be used to control the fan in the duct and make sure the pressure drop in the duct is not affecting the performance of the system.

The relative humidity sensors are especially important in this specific type of air handling unit. The relative humidity can be used to determine the moisture removal rate of the DW. Also, because of the nature of the SSLC technology, relative

humidity is extremely important. Multiple relative humidity sensors were placed at important points such as the process air outlet. Also, a relative humidity sensor was placed after the evaporator to ensure that only sensible cooling occurs over the evaporator and no moisture removal occurs.

The heater not only reconditions the air, but also serves the purpose of measuring the airflow rate. With all of the instruments in the air flow loops, all air side properties can be determined and cooling capacities can be calculated.

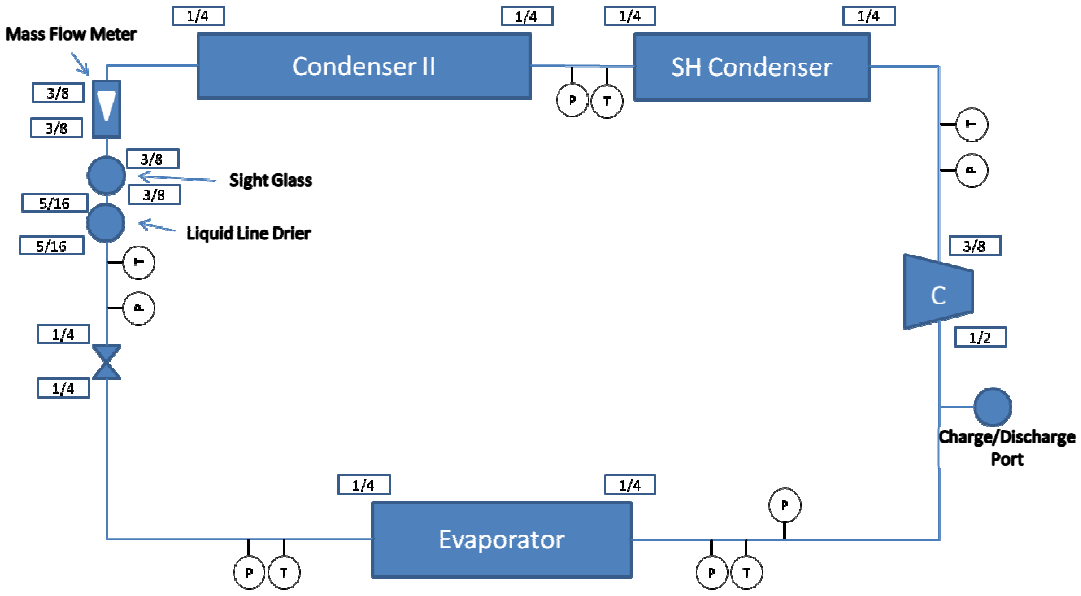

Figure 30 Refrigeration Loop Process Diagram

Figure 30 shows a more detailed refrigeration loop, including the instrumentation and additional necessary components in the refrigeration line.

Figure 30 also shows the refrigeration side instrumentation. All state points have thermocouples and pressure sensors. A mass flow meter was installed to determine the mass flow rate of the refrigerant. With the mass flow rate, temperature and

pressure at all state points, the remaining fluid properties can be determined as well as the capacities of the heat exchangers.

Chapter 4: Construction of Prototype and Test Facility

4.1: Overview

The experimental setup is broken down into three loops: the process side air loop, the exhaust side air loop and the refrigeration loop. Both air flow loops were built around the DW. The DW apparatus was built to provide the best possible air flow paths for both the process air and regeneration air. Figure 29 shows all three loops and the direction of flow. Within each loop, instrumentation is installed in order to best measure the required properties for observation and calculations of the performance of the system. The instruments are connected to a data acquisition module that interfaces with a computer program used to monitor and control the system.

4.2: Desiccant Wheel Construction

4.2.1: Desiccant Wheel Casing

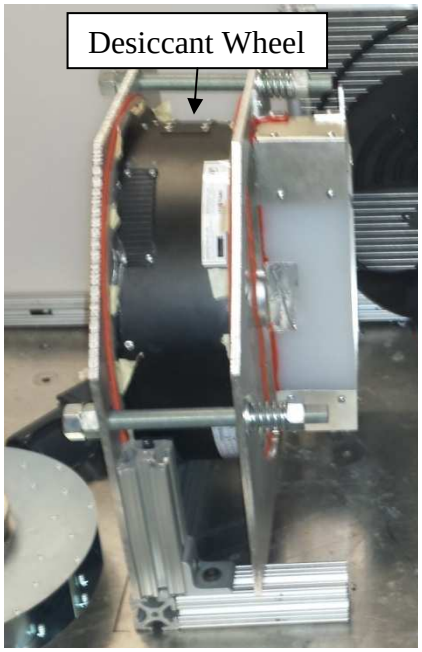

Figure 31: DW Casing Side View

Figure 31 shows a side view of the DW casing. The DW sits between two aluminum plates held together by threaded rods. The DW contacts the plates on two rubber gaskets covered in a low friction material in order to create the best seal, while still allowing for the wheel to turn freely. There are also three threaded rods tightened equally to ensure an even distribution of pressure on the wheel from both plates. The design for the plates provides the most leak tight method for the DW, while still allowing the wheel to turn unrestricted aided by a 12 W motor. In order to allow for the plates to seal properly, the larger support plate is mounted to the system, while the second smaller plate is free to move as the threads are tightened.

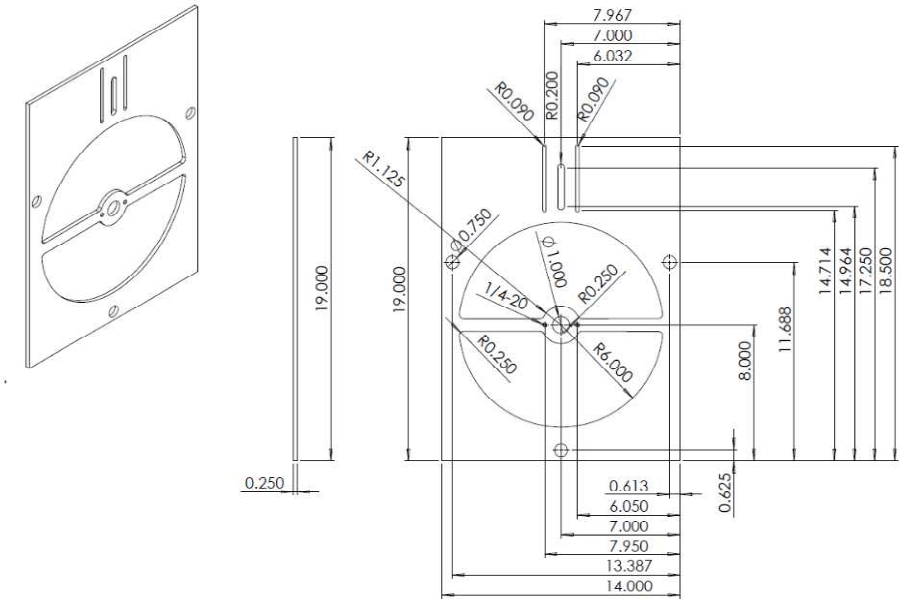

Figure 32: DW Plates CAD Drawing (inches)

Figure 32 shows the dimensioned drawing of the two aluminum plates designed for the DW casing. Due to the height constraints of the system, as well as the restricted depth of the system, the plates were designed at 356 mm by 483 mm, the smallest they could be while still providing enough space for the DW and motor to be mounted. At 356 mm tall, the plate only provides an inch of clearance for the

rubber gasket. Both plates were designed identically, but the second plate was later cut smaller to save space. Only the first plate requires the full 483 mm width in order to mount the motor. There is also a portion of the plate that separates the process air side and the regeneration air side. Once the plates were machined, any excess material was cut off in order to save as much space as possible.

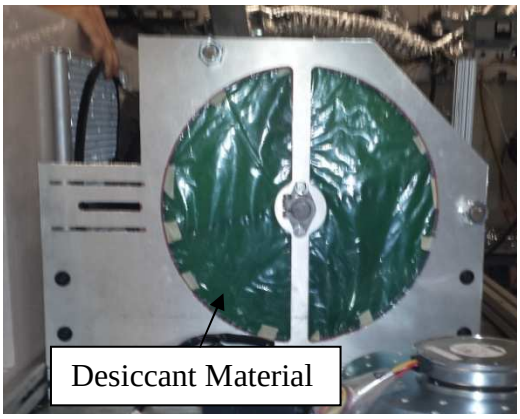

Figure 33: Final DW Plate

Figure 33 shows the final result after removing all excess material from the first DW plate. The top left corner of the plate was removed with the intention of putting in a bypass for the regeneration air when no dehumidification was required. The top right corner was removed to provide enough space for the evaporator fan duct. The three slots on the left side provide a spot for the motor to be mounted to the wheel. The second plate is identical to the first plate, except that the left side where the motor is mounted has been removed to provide space for the compressor.

4.2.2: Desiccant Wheel Air Flow Ducts

Only one air flow duct was required on the DW casing. The reason the other three openings remained fully open was to allow for the most unrestricted air flow through the DW.

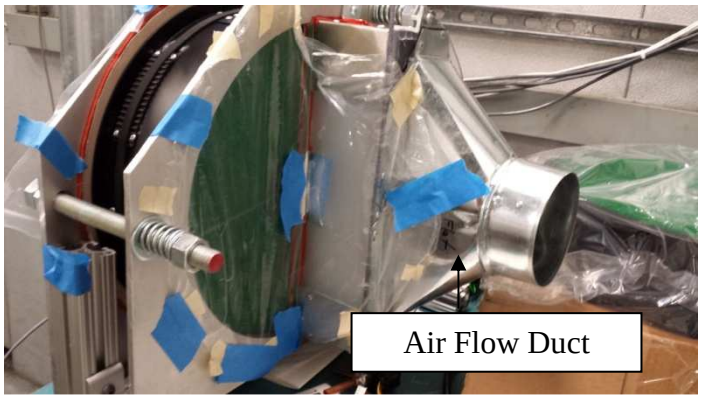

Figure 34: DW Front View

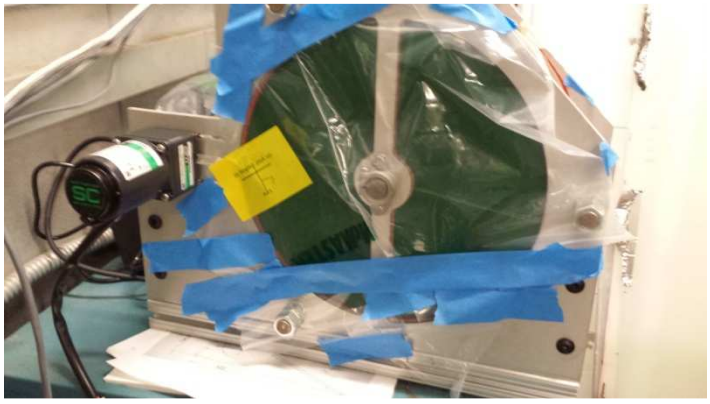

Figure 35: DW Back View

Figure 34 shows the DW front view which is the process air side inlet and regeneration air side outlet.

Figure 35 shows the back side of the DW which is the process air side outlet and regeneration air side inlet.

The process air side remains fully open to allow for the most unrestricted air flow path possible. It is important to also keep the inlet and outlet size similar to reduce the pressure drop. No additional ducting was necessary because the air can flow freely directly through the DW since there is no other path for the air to take.

Once the air exits the DW, it is immediately drawn into the centrifugal fan with no ducting required.

The regeneration side inlet is also completely open to allow the most unrestricted air flow through the wheel after flowing over the desuperheat condenser. No additional ducting was required, nor would any additional ducting help with the airflow path.

The regeneration side outlet required ducting as seen in Figure 34. It is important to keep the inlet and outlet size similar to avoid unnecessary pressure drop so the cross sectional area of the duct was slowly reduced to the size of the inlet to the desuperheat centrifugal fan. Because the air was being drawn through the DW, the DW regeneration side air flow needed to be ducted directly into the fan. A 76 mm section was constructed on the outlet of the regeneration side to allow for even flow before reducing the size of the duct.

4.2.3: Desiccant Wheel Motor

The DW motor is a 12 W manually controlled motor that runs the wheel anywhere between 1-10 RPM. The power consumption of the motor is negligible in comparison to the fans and the compressor. Because regeneration is done reutilizing waste heat, and the motor is so small, the additional 1 kW of latent cooling done by the DW only increases the capacity without increase the power consumption.

Figure 36: DW Motor

The DW motor was mounted in a position where it created the smallest footprint for the DW apparatus. By mounting the motor towards the inside of the two plates, there was more room on the other side for the desuperheat condenser. The motor was mounted using threaded steel rods to support the weight of the motor ad well as provide stability while the motor turns the wheel. The motor can also be manually controlled to change the speed of the wheel depending on the moisture removal rate of the wheel.

Figure 37: DW and Motor Connection

A belt was use to drive the DW with the motor. The side mounted motor connected by the belt allowed for the motor to turn the DW without being in the way of either air flow path. Strips of belt teeth were attached along the DW as seen in

Figure 37. The belts were aligned and then tension was put on the belt. Once tension was put on the belt, the motor was tightened to the plate. The DW was then tested to ensure the plates were not too tight and the teeth on the belt would catch and not skip.

4.3: Process (Space) Side Air Loop

The process air side loop was tight and complicated. There were four main parts of the process air side loop; upstream of the DW, downstream of the DW, the DW bypass and the process air side duct outside of the main unit.

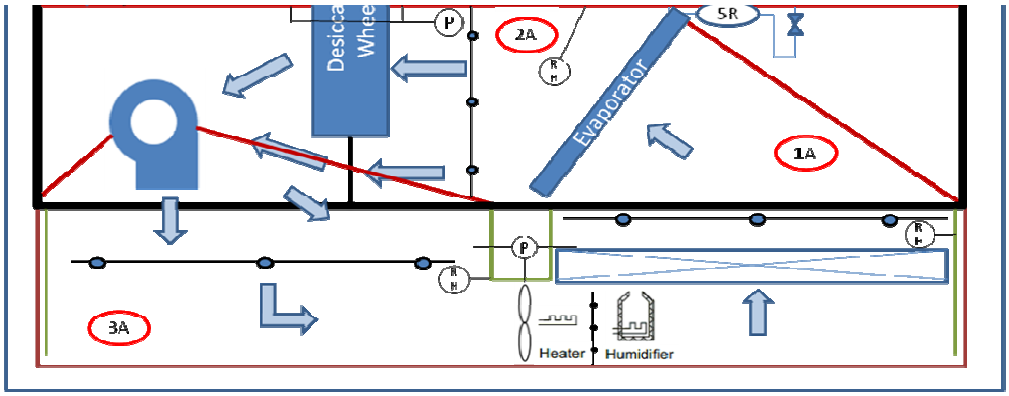

Figure 38: Process Air Side Loop Diagram

Figure 38 shows the schematic for the process air side loop. The bold line represents the PTAC unit and the thinner line below the bold rectangle represents the process air side duct.

4.3.1: Upstream of Desiccant Wheel

Upstream of the DW is the evaporator. The evaporator is angled to create a better flow path for the air between the evaporator and the DW.

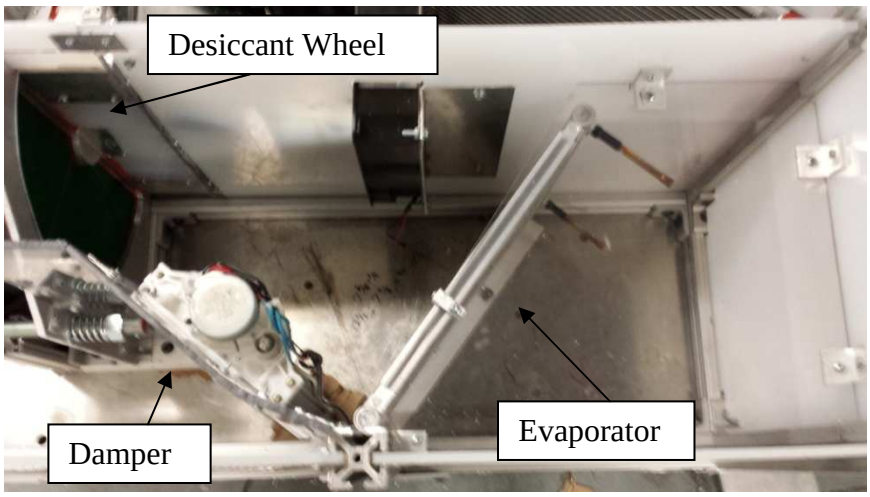

Figure 39: Process Air Side Loop Upstream of DW

Figure 39 shows the chamber upstream of the DW. Due to space constraints, the desuperheat fan is partially in the process air side path, but does not cause any

issues with air flow patterns. The damper also shown in Figure 39 is partially in the air flow path of the process air but also has negligible effects on the air flow pattern. The damper is angled due to the space constraints, which does cause some pressure drop as well. This pressure drop caused by the sharp turn into the damper in a bypass case is negligible compared to the pressure drop across the DW.

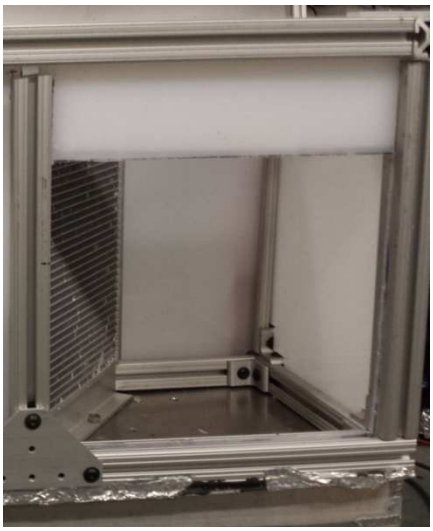

Figure 40: Process Air Side Inlet

Figure 40 shows the inlet to the process air side during construction. The inlet is the same size as the evaporator, allow for the best possible air flow over the evaporator.

The upstream chamber also contained the expansion valve. An electronic expansion valve was used in order to have better control of the system.

Figure 41: Electronic Expansion Valve

Figure 41 shows the electronic expansion valve (EXV). The EXV can be seen in Figure 38 as well, immediately next to the evaporator. It was also shown that a wall separates the evaporator and the EXV, but for the purpose of testing, the wall was left out to allow access to the EXV. The additional wall in the upstream of the process air side could have a positive effect on the air flow, reducing the pressure drop and power consumption.

The upstream chamber also contains a relative humidity sensor and a thermocouple grid immediately after the evaporator.

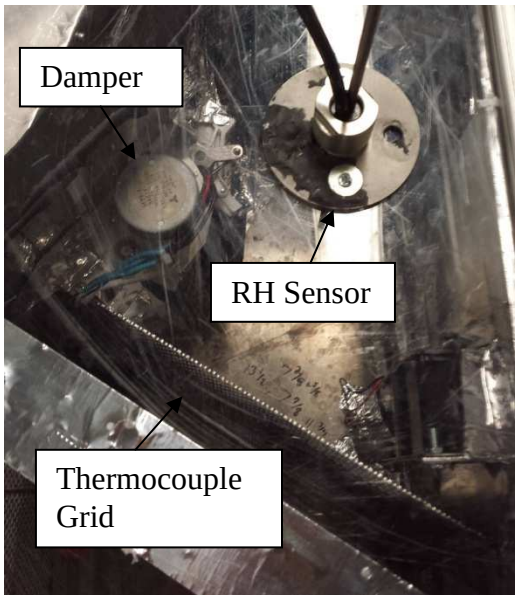

Figure 42: Thermocouple Grid and RH Sensor

As shown in Figure 42, the thermocouple grid is the same size as the face of the evaporator, and the relative humidity sensor sits in the center of the air flow. These two instruments are important for multiple reasons. By measuring the temperature after the evaporator, the heat transfer between the air and the evaporator can be determined. If the temperature is too high or too low the expansion valve or air flow rate can be adjusted depending on the issue.

The RH sensor is also important in order to determine whether or not any latent cooling occurs over the evaporator. Only sensible cooling should occur over the evaporator, so the air flow rate or the expansion valve can again be adjusted. The RH sensor is also used to determine the moisture removal rate of the DW along with the RH sensor after the DW.

4.3.2: Downstream of Desiccant Wheel

The chamber immediately downstream of the DW is empty and free of any unnecessary obstructions.

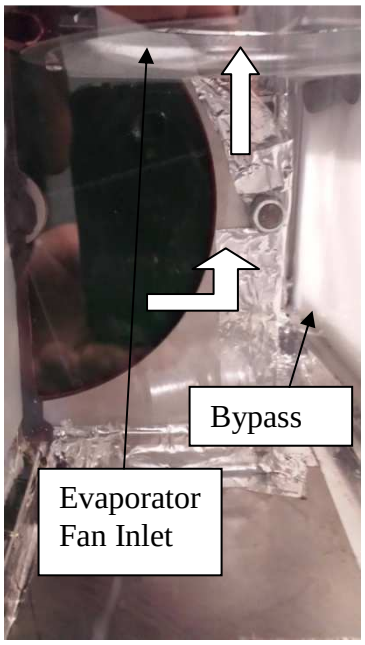

Figure 43: Chamber Downstream of Desiccant Wheel

The air flows out of the DW and is drawn into the centrifugal fan through the nozzle seen in Figure 43. On the right side of the figure the narrow bypass can be seen alongside of the DW casing. In the same manner, the air flows through the bypass into the chamber and is drawn into the centrifugal fan through the inlet nozzle in the top of the chamber. The chamber is left open instead of the DW being directly ducted into the fan due to the necessity of the bypass.

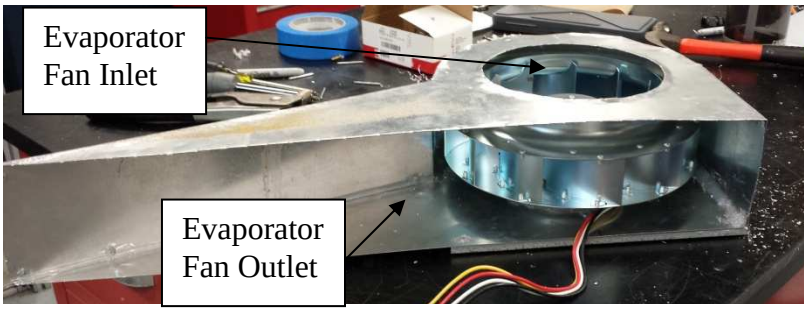

Figure 44: Centrifugal Evaporator Fan Duct

Figure 44 shows the centrifugal fan duct completed. The duct needed to be specially made due to custom sized casing required around the fan. The duct channels the air flow only out of the front half of the fan and restricts the flow of air in any other direction. The duct also opens up into a wider outlet to match the size of the preexisting PTAC unit outlet. The duct was constructed using aluminum sheets. But the fan is mounted to a 7 mm thick aluminum plate to stabilize the fan due to its high rotational speeds. The hole in the bottom of the duct (on top in Figure 44) is the fan inlet. It was important that the inlet to the duct be as close as possible to the inlet of the fan without the parts rubbing to ensure an airtight system. With too large of a gap, the air will just recirculate and the performance of the fan will diminish. Additionally, an inlet nozzle ring was used to increase the performance of the fan as well.

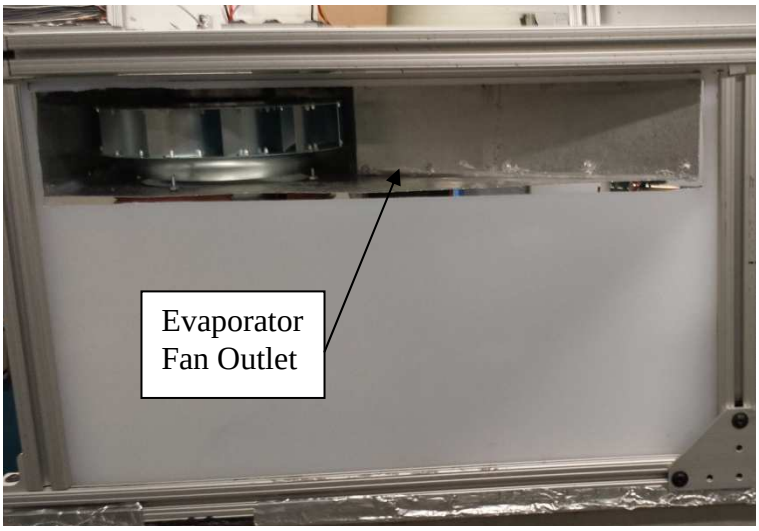

Figure 45: Process Air Side Outlet

Figure 45 shows the process air outlet. The evaporator fan and duct are mounted to frame of the system to ensure no vibrations or additional noise from the fan. The outlet dimensions are 102 mm in height by 635 mm in length, equal to the outlet of the standard PTAC unit. The centrifugal fan has the additional bonus of reducing the pressure drop. The tight 180 degree turns have high pressure drops associated with them. Because the inlet of the evaporator fan is not in the same plane as the outlet, the fan can turn the air 90 degrees up and 90 degrees out without the higher pressure drop. The centrifugal fan was also used because of its high pressure lift as well as high air flow rate capabilities. No instrumentation was implemented immediately downstream of the desiccant. All instruments measuring air properties after the DW were in the process air side duct immediately after the process air side outlet.

4.3.3: Air Flow Damper for DW Bypass

The DW bypass damper is manually controlled and can be opened, closed and partially opened. The damper sits next to the DW as an alternative air flow path to the DW.

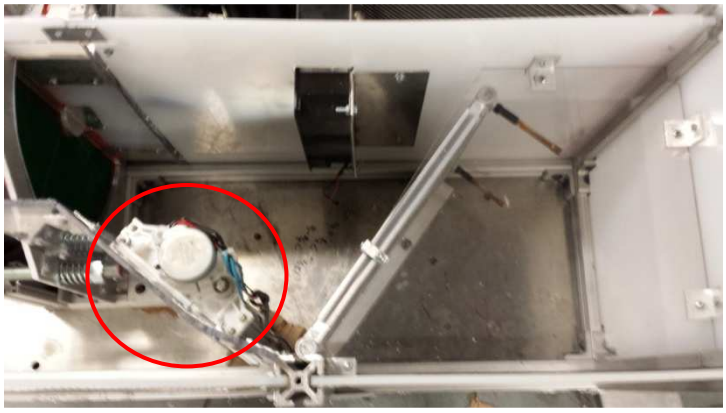

Figure 46: Air Flow Damper for DW Bypass

Figure 46 shows the placement of the DW in the process air side path. The damper separates the upstream and downstream chambers completely isolating them from each other. When the damper is closed the entire air flow is through the DW. The DW is sufficiently leak tight to prevent air taking the path of least resistance and bypassing the DW.

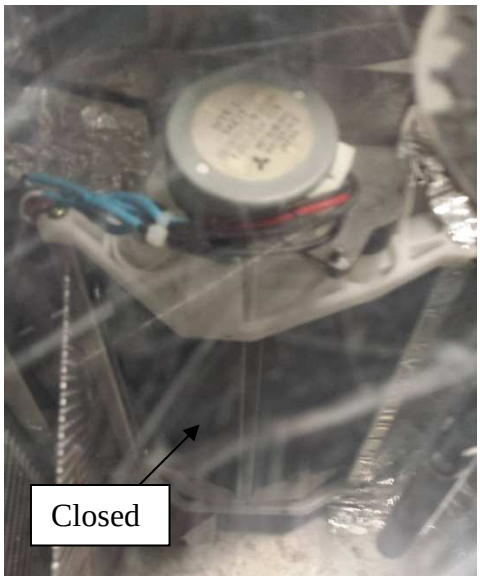

Figure 47: Damper Closed Position

Figure 47 shows the damper in the closed position. The damper is sealed by foam, creating a sufficiently leak tight seal. The motor used to run the damper is on the magnitude of 4 W and is not constantly running so the power input is negligible.

Figure 48: Damper Fully Open Position

Figure 48 shows the damper is the fully open position. In this case most if not all of the air flow goes through the damper and bypasses the DW. The purpose of this operating condition is when air needs to be cooled, but not dehumidified. By bypassing the DW when no dehumidification occurs, the pressure drop through the DW is also bypassed, decreasing the power consumption of the evaporator fan. When no additional humidity load is introduced to the space, the SSLC unit can operate for long periods of time in the "dry cooling case" bypassing the DW and increasing the COP even higher during these hours of operation.

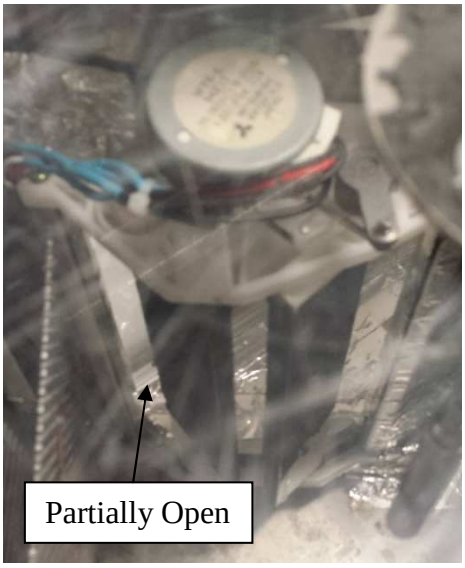

Figure 49: Damper Partially Open Position

Figure 49 shows the damper in a partially open position. The damper can be manually opened to any point, not just opened or closed. The purpose of partially opening the damper is to adjust the amount of moisture removed through the DW. Using the RH sensors, thermocouple grids and air flow rate, the moisture removal rate can be calculated. In order to meet the cooling capacity of the evaporator, there is a high rate of air flow. Too high of an air flow rate through the DW could remove

too much moisture, making the air too dry and thermally uncomfortable. By adjusting the damper and allowing some of the air to bypass the DW, the required moisture removal rate and latent load can be met. During testing, the required latent load would be determined by adjusting the damper manually until the design point is met.

4.3.4: Process Air Side Duct

The process air side duct is not part of the PTAC unit. The duct's purpose is to represent the space being cooled. The process air side duct must also be large enough to reheat and rehumidify the air to the required inlet condition.

Figure 50: Process Air Side Duct

Figure 50 shows the completed process air side duct. The air first flows out of the PTAC unit over the RH sensors and through a thermocouple grid. Next, the air is rehumidified and then drawn through the fan. The air temperature is measured in another thermocouple grid and then reheated over an electric heater. Finally, the air flows through an air mixer, over another thermocouple grid and back into the PTAC inlet.

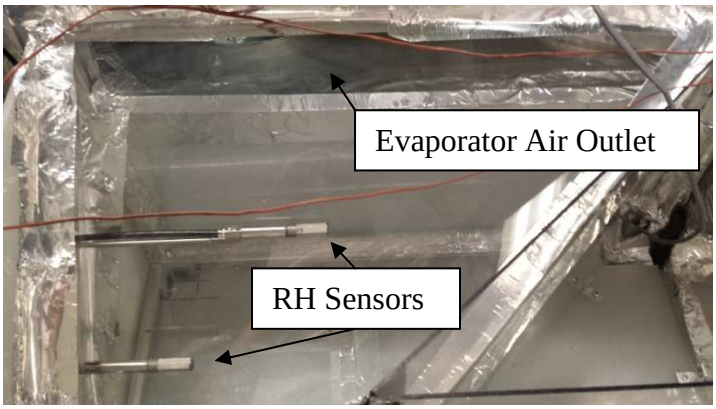

Figure 51: Process Air Duct with RH Sensors

Figure 51 shows the point where the air immediately exits the PTAC unit and flows over the two RH sensors. Two RH sensors are used to increase the accuracy of the humidity related calculations at this point since dehumidification is significantly important in this technology. This is the point where the humidity after the DW is measured so it is used to calculate the moisture removal rate and latent cooling capacity. At this point in the duct, the air is channeled from a wide and short inlet to a smaller square outlet for the air to be processed.

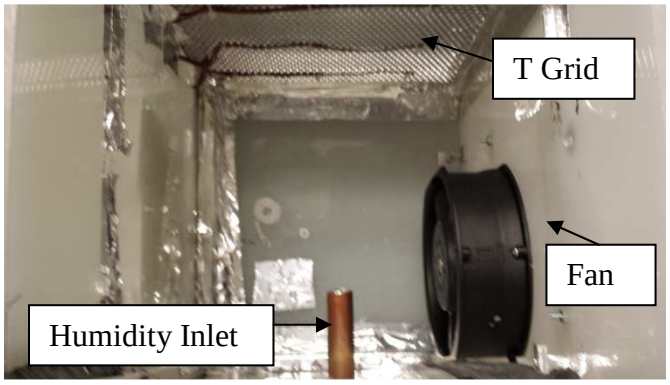

Figure 52: Process Air Duct with Rehumidifcation and Pressure Balancing Fan

Figure 52 shows the next portion of the process air side duct. The copper tube at the bottom of the figure is connected to the humidifier of the environmental

chamber. The temperature is measured over the thermocouple grid before the humidity is added. The cool humid air is then drawn through the fan. The fan is used to balance the pressure over the duct. The duct does another 180 degree turn so there will be a significant pressure drop over the duct. When the differential pressure is zero over the duct, then the duct will not have an adverse effect on the performance of the PTAC unit. As shown at the top of the figure, the inlet of this section is square after it has been ducted down from the wide and short PTAC unit outlet.

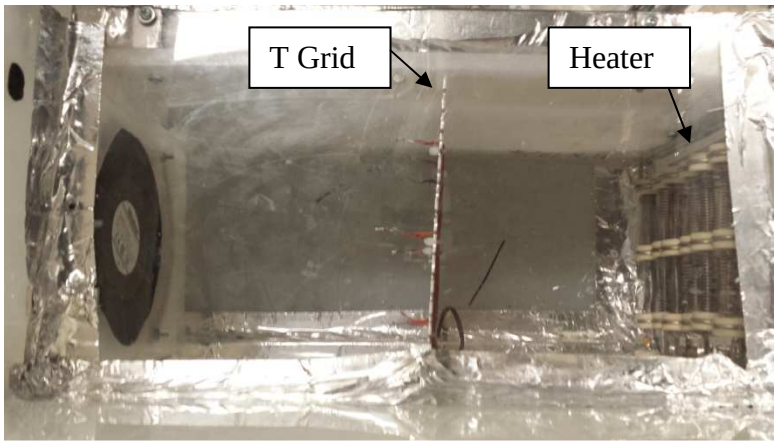

Figure 53: Process Air Duct with Electric Heater

Figure 53 shows the third portion of the process air side duct. The temperature of the air is measured again after humidification which should add some heat before adding heat from the electric heater. The air is mixed in the fan so an air blender or mixer is not necessary for accurate temperature readings. The electric heater will reheat the air to the space inlet conditions.

The heater can also be used as an air measurement device. The amount of heat being added to the system is known based on the power consumption of the heater. By knowing the properties of the air before and after the heater and the heat input by the heater, the mass flow rate of the air can be calculated. Without

additional components in the system, this is the most accurate method of measuring the air flow rate.

Figure 54: Process Air Duct with Mixer and PTAC Inlet

Figure 54 shows the final section of the process air side duct. After reheating the air, the air flows through a mixer to evenly distribute the temperature of the air. Without the mixer, the air would have an uneven temperature distribution and a less accurate temperature reading would be taken. Using the mixer increases the accuracy of the readings over the thermocouple grid and removes unnecessary uncertainty. The duct was constructed to allow for 204 mm of duct upstream of the mixer and 102 mm of duct downstream of the mixer. These upstream and downstream distances are necessary based on the air flow rate in order to ensure proper mixing based on manufacturer's data.

4.4: Exhaust Air Side Loop

The exhaust air side loop consists of two separate inlets combining into one common outlet. The first half of the loop is the desuperheat condenser loop. The second half of the loop is the condenser II loop. The exhaust loop is similar in design to the standard PTAC unit exhaust loop. The air only crosses the boundary of the back of the PTAC unit. The air comes in through the sides of the back and exits through the middle of the back of the unit. Similar to the evaporator loop, the 180 degree turn creates a poor air flow pattern but it is necessary for the PTAC design. Figure 5 shows the standard PTAC unit exhaust air flow.

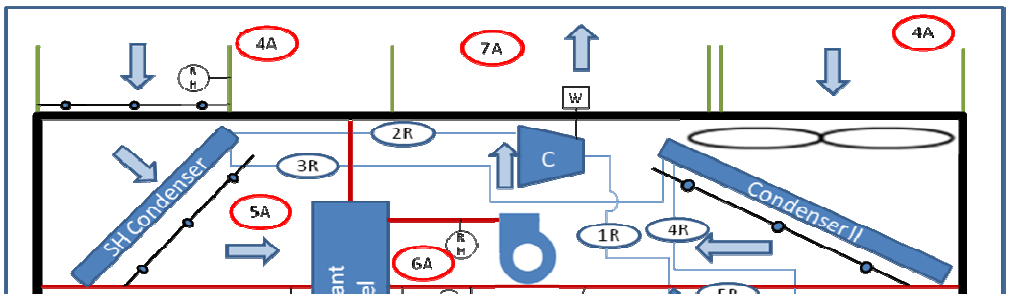

Figure 55: Exhaust Air Side Loop Diagram

Figure 55 shows the process schematic of the exhaust air loop. In the diagram, the bold line represents the PTAC unit and the lighter line represents the environment at ambient conditions.

4.4.1: Desuperheat Condenser Loop

The desuperheat condenser loop has an upstream and downstream of the DW side, but is simpler than the evaporator process air side. Originally, a bypass was planned for the desuperheat condenser loop, but the complexity of the ducting was

disproportional to the energy savings. Because the desuperheat fan does not consume as much energy as the other fans, there was a negligible benefit to incorporating a bypass.

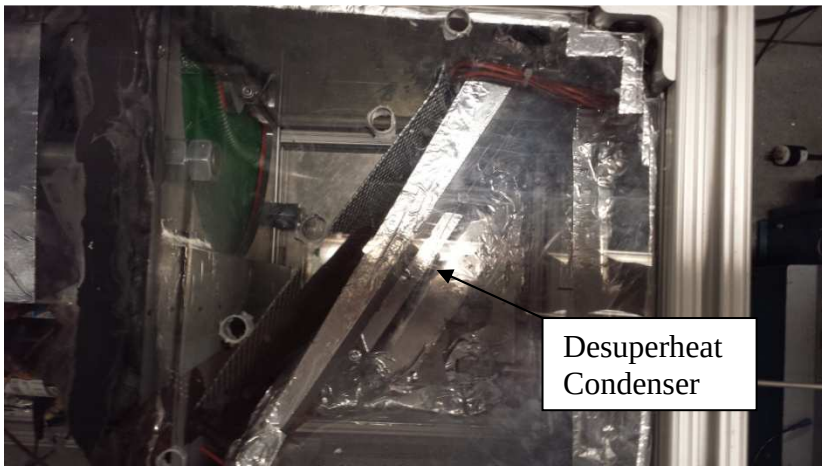

Figure 56: Desuperheat Condenser Loop Upstream of the DW

Figure 57: Desuperheat Condenser Loop Inlet

Figure 56 shows the upstream section of the desuperheat condenser loop. Air enters through the inlet seen in Figure 57 through a thermocouple grid and over an RH sensor. These sensors are in the flow path at this point to validate the chamber's set ambient conditions.

The air flows over the desuperheat condenser and is heated to the required regeneration temperature. The temperature is measured at the next thermocouple grid immediately after the condenser. The DW is left completely open to allow for the maximum airflow through the wheel after the condenser. The condenser is angled in order to create the best air flow pattern possible. Directional fins can be placed on the inlet to channel the air at the angle of the condenser to maximize air flow. These fins would also help separate the inlet air from the exhausted air in the middle of the back of the unit.

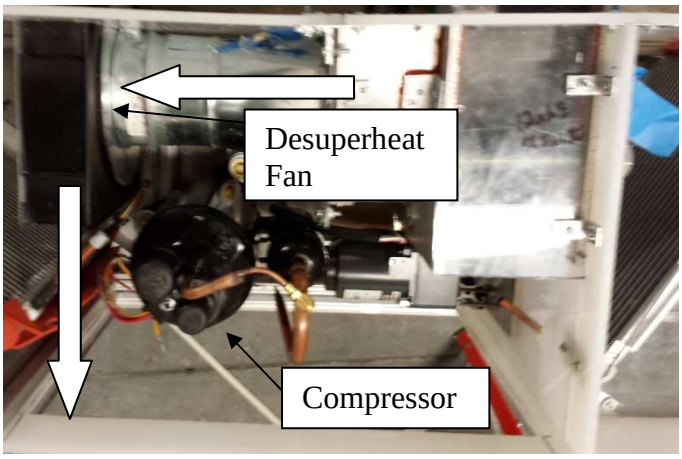

Figure 58: Desuperheat Condenser Loop Downstream of the DW

Figure 58 shows the airflow path of the desuperheat condenser loop downstream of the DW. The air is ducted directly out of the DW and channeled into

the centrifugal fan. The centrifugal fan blows out the air to the environment through the common outlet in the center of the unit.

4.4.2: Condenser II Loop

The condenser II loop is the most similar to the original PTAC unit.

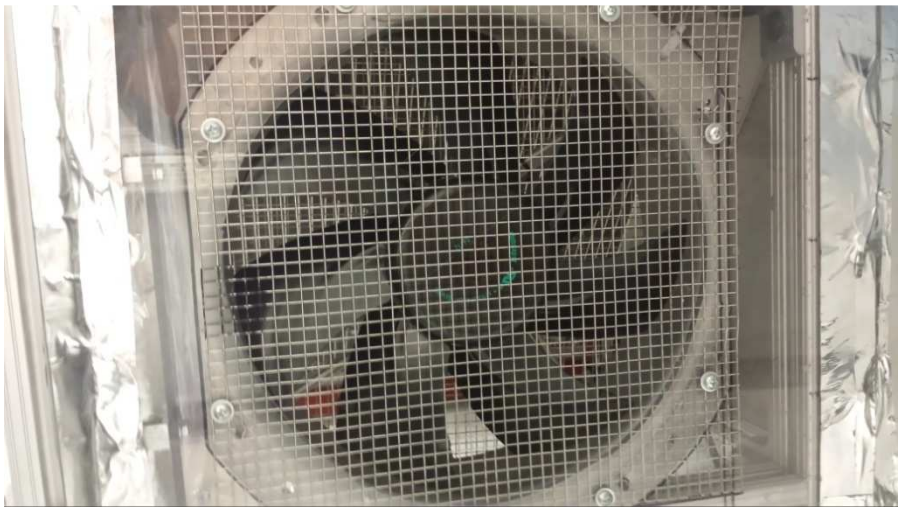

Figure 59: Condenser II Loop Inlet

Figure 59 shows the inlet to the condenser II loop. The condenser II fan draws air in directly from the environment and cools the condenser II. Similar to the desuperheat inlet, the condenser II inlet is on the side of the back of the unit. The air could be channeled using fins to better separate the ambient air and the exhausted air out of the middle of the back of the unit. Unlike the other two air flow paths, the condenser II does not draw the air over the heat exchangers. Instead it draws air from the environment and blows the air over the condenser II.

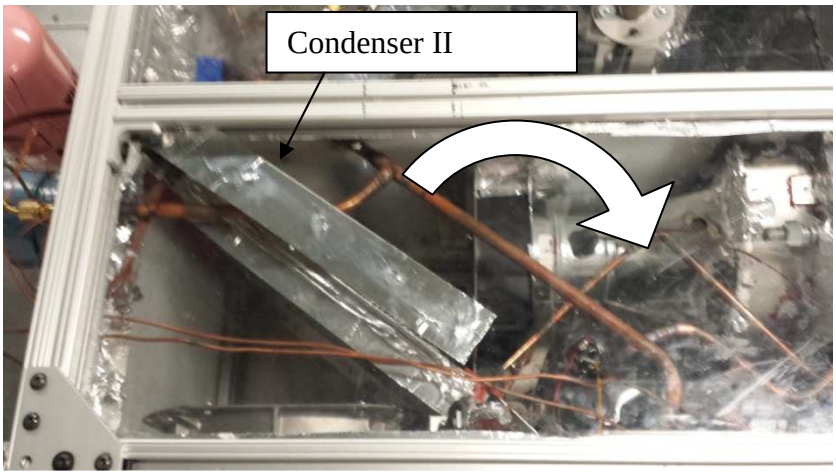

Figure 60: Condenser II Air Flow Path

Figure 60 shows the air flow path through the unit. It is obviously very tight which creates a larger pressure drop. Also, immediately in front of the condenser is the desuperheat fan with could cause an uneven air flow distribution over the condenser II. In this case, the condenser II was angled due to space constraints. The condenser II is larger than the other two heat exchangers creating a more difficult air flow pattern. A thermocouple grid is placed immediately after the condenser II to ensure cooling is being done as well as to validate the VapCyc model.

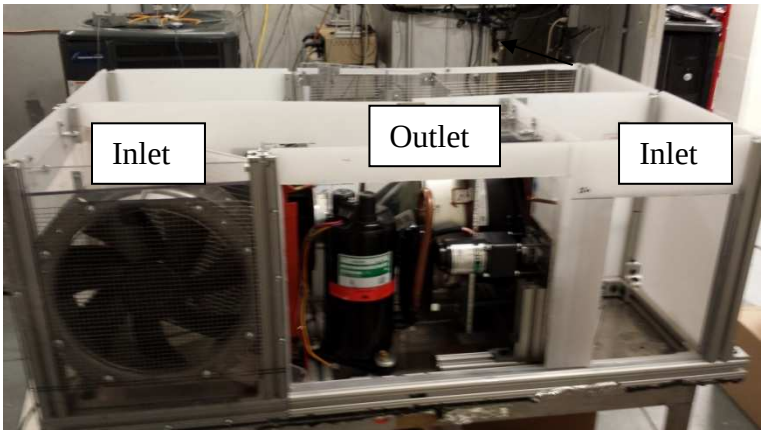

Figure 61: Inlets and Outlets of Condenser Side Air Streams

Figure 61 shows the back side of the PTAC unit. The backside is open directly to the environmental chamber which is set for the required ambient test conditions. The two inlets are on either side of the common outlet. Another important design choice is the placement of the compressor. The compressor sits in the exhaust air flow path. The exhaust air cools the compressor, increasing the efficiency of the compressor.

4.5: Refrigeration Loop

Figure 30 shows the refrigeration process diagram. The main components of the refrigeration loop were constrained to the inside of the PTAC unit to validate the space requirements. Larger components that would not be in the final product such as the mass flow meter were connected on the outside of the unit. A liquid line drier and a sight glass were connected in the refrigeration line to remove liquid from the system at points were vapor only was necessary and to ensure there was no water in the system.

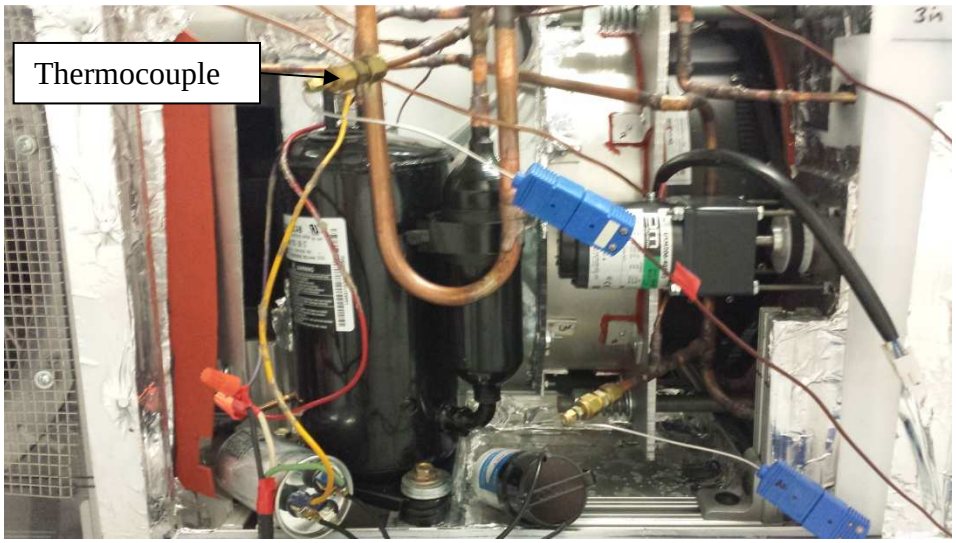

Figure 62: Refrigeration Line Connections

Figure 62 shows some of the refrigeration line connections between the expansion valve, evaporator, compressor and the two condensers. All tubing was constructed outside of the system so only final brazes to the large components needed to be done within the system due to the space restrictions. Differently sized connections were made depending on the component inlets and outlets. Figure 30 shows the connection sizes of the large components.

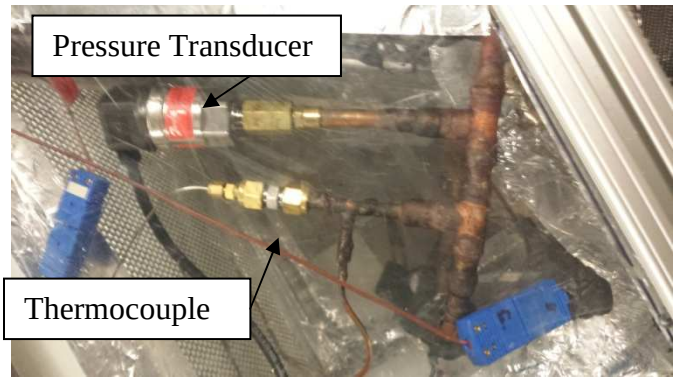

Figure 63: Refrigeration Line Instrumentation Points

Figure 63 shows an example of an instrumentation point within the refrigeration loop. Each state point in the VCS has a instrumentation point to measure the temperature and the pressure. A thermocouple is inserted all the way down the tube into the refrigeration flow stream. Also on the instrumentation point is a connection to a capillary tube that is connected to a pressure transducer. The capillary tubes allow for the transducers to sit further away from the point being measured, reducing the clutter within the system.

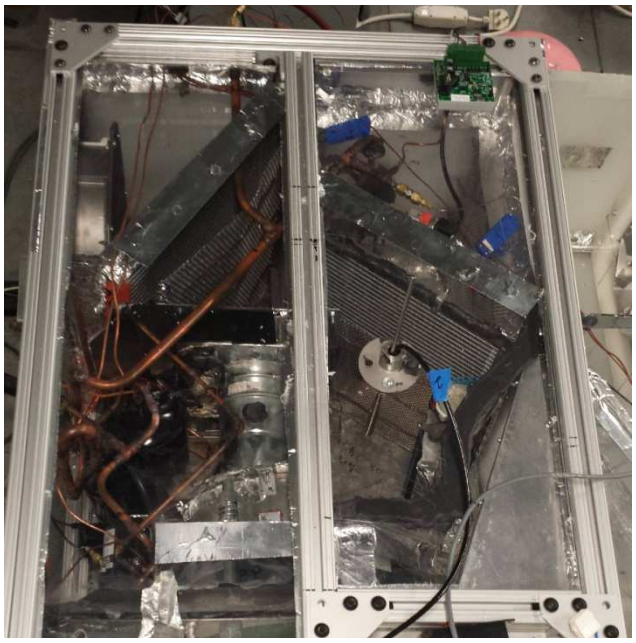

Figure 64: Overview of Refrigeration Line

Figure 64 shows a top down view of the entire PTAC unit where the refrigeration line in the system can clearly be seen. There are more lines running through the system than a standard PTAC unit due to the additional condenser, as well as the placement of the evaporator and the desuperheat condenser. Because the two flow paths through the DW must flow opposite each other, the process air heat exchanger (evaporator) and the regeneration air heat exchanger (condenser) must sit at opposite corners of the unit. This creates a much larger distance the refrigeration loop must cover.

4.6: Instrumentation

The instrumentation used in the setup can be broken down into three categories: air side instruments, refrigerant side instruments, electrical device measuring instruments. All instrumentation was calibrated using a spread of known values and comparing them to the signal output of the instrument. Then, an equation

was set for each individual instrument based on the results of the calibration to reduce the error in the instruments. The instruments were calibrated within the system to further reduce any error in signal or the data acquisition (DAQ) module. Because the instruments were calibrated, the accuracy was taken as the manufacturer's rating.

Table 8: Specification of Instruments

Instrument	Type	Manufacturer	Model #	Range	Accuracy
Pressure	Strain	Setra	280E/280E	0–34.47/ 0-68.95 bar	±0.11% f.s.
Differential Pressure	Strain	Setra	2641001WD11T1G	0 – 1" W.C.	±1.0% f.s.
Thermocouple	T-type	Omega	N/A	-250 to 350°C	±0.5°C
Mass Flow Meter	Coriolis	Micro Motion	R025	0-100 g/s	±0.25% f.s.
Relative Humidity	Capacitance	Vaisala	HM310	0 – 100 %RH	±1.0% RH
Watt Meter (Compressor)	Watt Transducer	Ohio Semitronics	GH-0200	0 – 4 kW	±0.2% f.s.
Voltage Meter	DC Voltage Transducer	CR Magnetics	CR5310-50	0-50 VDC	±0.5% f.s.
Current Meter	DC Current Transducer	CR Magnetics	CR5211-10	0-10 ADC	±1.0% f.s.

Table 8 summarizes all instrumentation used in the test facility. All instruments were chosen to provide accuracy in readings as well as further calculations.

4.6.1: Pressure Measurement

Three models of pressure transducers were installed in the system. The first two models were strain type pressure transducers installed in the refrigeration line at all state points. Capillary tubes were installed at the points being measured so that the pressure transducers could be installed outside of the already confined spaces. Two

models with different ranges were chosen for the high and low side pressures for the best accuracy. Three 0-34.47 bar pressure transducers were installed on the low side and two 0-68.95 bar pressure transducers were installed on the high side.

The third model was a strain type differential pressure transducer on the air side. The differential pressure transducer was used to monitor the system and was not used in data analysis. The differential pressure was maintained at zero through the process side air duct to avoid unnecessary pressure drop that would need to be overcome by the evaporator fan. Another fan was used in conjunction with the differential pressure transducer to reduce the pressure drop of the duct to zero.

4.6.2: Temperature Measurement

All thermocouples used were T-type thermocouples calibrated in a temperature bath. Thermocouples were used in both the refrigeration side and air side loops. Thermocouple probes were inserted into the refrigeration flow at each of the five state points.

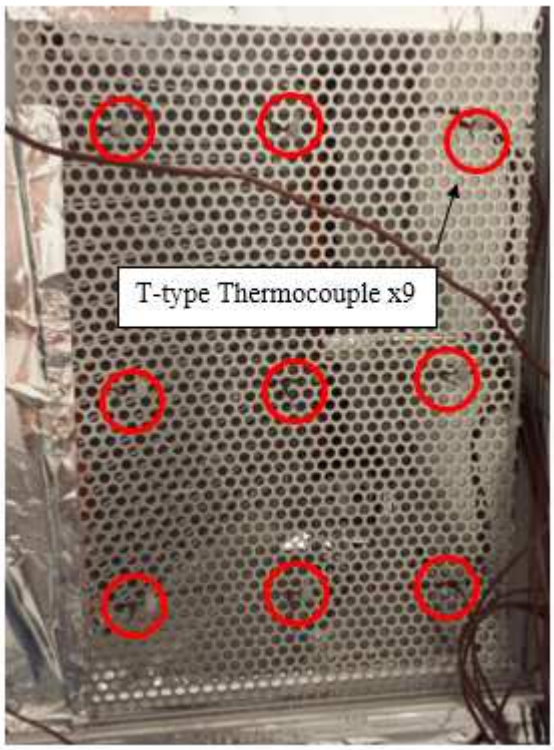

Figure 65: Thermocouple Grid

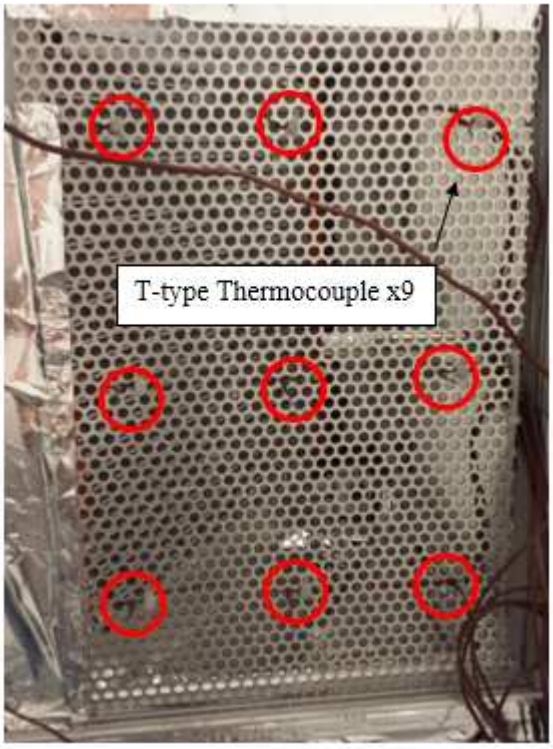

Figure 65 shows the layout of the thermocouple grids used for air side temperature readings. Nine thermocouples were evenly distributed over the face of the grids and all grids were sized based on the cross flow area of the duct where they were being installed. At most points, all nine thermocouples were combined and averaged for a single data point. At the system outlet and the desuperheat condenser outlet, more accurate temperature profiles were necessary, so horizontal rows of three thermocouples were averaged instead.

4.6.3: Mass Flow Measurement

The mass flow meter installed in the test loop is a Micro-Motion R025 with a rated accuracy of 0.25 g/s. After calibration of the device, the accuracy was taken as the manufacturers rating.

Figure 66: Mass Flow Meter

Figure 66 shows the external installation of the mass flow meter. The mass flow meter was installed outside of the system due to its size and the fact that it's a part of the test facility, but not the manufacturable end product.

4.6.4: Relative Humidity Measurement

Due to the nature of the system, relative humidity data analysis was extremely important. Six relative humidity sensors were installed in the system at different air side state points. They were installed directly in the center of the air flow in order to ensure accuracy. Also, at the process air outlet, two humidity sensors were used to increase the accuracy of the entire flow.

4.6.5: Power Measurement

Two separate methods of power measurement were used for the compressor and the fans. The compressor was connected to a wattmeter in order to measure the power consumption of the compressor.

Each of the fans was individually connected to a voltage transducer and a current transducer. The use of both of these instruments could then be used to solve for the power consumption of each of the fans.

It was important to monitor the power consumption of each components individually instead of the power consumption of the entire system as a whole. Because the fans are variable speed and still are being sized, it is important to know the individual power consumption of each fan in order to reduce power consumption as a whole and increase the COP.

4.6.6: Air Flow Measurement

Air flow measurements were taken using multiple methods, and then compared to validate each separate method. The first method of air flow measurement was done early in testing to get a rough estimate of the air flow rate of each fan. An air flow anemometer was used to calculate the velocity which was then

used to calculate the air flow rate through the cross sectional area of the flow path. This was not the most accurate method of air flow testing but was used as a checkpoint to ensure the fans were sized properly and there was an even distribution of air over the heat exchangers.

The second method of calculating the air flow rate was through the use of the heater in the system. Because of the size of the heater, the heat input into the air flow was known and the temperature could be measured before and after the heater. An energy balance was used to determine the air flow rate. Similarly for comparison, the same method was used with the refrigerant side calculation of the evaporator capacity. Both of these values could then be compared for accuracy.

4.7: Data Acquisition System

All sensors and controlled devices were connected to a bank of Field Point modules manufactured by National Instruments and installed near the test system. These modules allow for remote collection of data and remove the necessity to run a large number of connections directly to the data acquisition computer, reducing error in the measurement from voltage drop through long signal wires.

Data collection, analysis, and system control were accomplished with a Virtual Interface (VI) programmed using the commercially available LabView software integrated with a refrigerant properties routine, RefProps.

4.8: Uncertainty Analysis

The uncertainty was calculated for all measured and calculated variables. The total uncertainty for measured values is the sum of the systematic error and the random error shown in the following equation.

$$u_{tot} = u_{sys} + u_{STD} \tag{24}$$

Where:

u_{tot} = total uncertainty of a measured value

u_{sys} = systematic uncertainty of a measured value

u_{STD} = random uncertainty of a measured value (one standard deviation)

The random uncertainty can be calculated as one standard deviation of the measured variable away from the collected data set as shown in the following equation.

$$u_{STD} = \sqrt{\frac{1}{N-1}\sum_{j=1}^{N}\left(x_j - \bar{x}\right)^2} \tag{25}$$

Where:

N = number of data points in the collected data set

j = data point index

x_j = measured variable data point at index j

$\bar{x}$ = average of the measured variable over the entire data set

The systematic uncertainty of a calculated variable is calculated using the systematic uncertainty of each of the measurements involved in the calculation. The

Pythagorean summation of uncertainties method is used shown in the following equation.

$$u_F = \sqrt{\left(\frac{\partial F}{\partial v_1} * u_1\right)^2 + \left(\frac{\partial F}{\partial v_2} * u_2\right)^2 + \left(\frac{\partial F}{\partial v_i} * u_i\right)^2} \quad (26)$$

Where:

F = calculated variable

u_F = uncertainty in the calculated variable "F"

u_i =uncertainty of the measured variable

v_i = measured variable

i = number of variables used to calculate "F"

Similar to the total measured uncertainty, the total calculated uncertainty is the sum of the calculated systematic and random uncertainties. Table 9 summarizes the typical values for the measured and calculated systematic, random and total uncertainties. The systematic uncertainties will remain constant throughout all data analysis, but the random uncertainty is subject to change based on data points collected and each test run.

Table 9: Typical Variable Uncertainties

Variable	Units	Systematic	Random	Total
Measured				
Refrigerant Temperature	°C	0.500	0.409	0.909
Refrigerant Pressure (high)	kPa	7.585	18.533	26.117
Refrigerant Pressure (low)	kPa	3.792	5.404	9.195
Mass Flow Rate	g/s	0.250	0.046	0.296
Air Temperature	°C	0.500	0.091	0.591
Relative Humidity	%	1.000	0.780	1.780

Voltage	V	0.250	0.005	0.255
Current	A	0.100	0.006	0.106
Compressor Power	W	8.000	9.828	17.828
Calculated				
Fan Power	W	2.560	0.308	2.868
Cooling Capacity (Air)	kW	0.405	0.033	0.438
Cooling Capacity (Ref)	kW	0.045	0.022	0.067
Air Flow Rate	m^3/h	94.960	29.899	124.859
Pressure drop	kPa	10.730	1.870	12.600

4.9: Shakedown Testing

Shakedown testing was done in two parts. First, the air side needed to be tested to ensure all fans were operational and controllable. The air side needed to be completed before the refrigeration line could run. In addition to testing all of the fans, the DW and the damper, it was important that the unit be leak tight. All fans were run at full capacity and the system was checked for air leaks. Any points leaking air would throw off the energy balance of the system. At full capacity, all leaks were very apparent.

After the air side was operational and leak tested, the refrigeration side needed to have shakedown testing performed. The first step in the shakedown testing was to charge the system with 200 grams of refrigerant. The compressor was turned on and the pressures were observed to see a difference in high side and low side pressure. Next, the expansion valve was tested to ensure superheating and subcooling could be achieved. Then, the system was charge with more refrigerant until the superheating and subcooling reached the ideal point and remained steady. The results of the shakedown testing were then used to calculate the capacity of the VCS alone.

Chapter 5: Results and Discussion

5.1: Air Flow Patterns Across the Heat Exchangers

Before construction of the refrigeration cycle began, testing was done on the air flow paths of the system. Due to the restricted air flow paths, obstructions within the air flow paths and significantly large pressure drops due to paths and the DW, it was important to study the air flow paths and make adjustments to the unit. Air flow testing was done using an air flow anemometer. The velocity was taken at different points at different heights over the three heat exchangers to observe the distribution of air flow. Also, the average velocity was taken and used with the surface area to determine the volumetric flow rate of each loop.

5.1.1: Evaporator

Air flow testing of the evaporator was done with the damper both closed and opened. When the damper was closed, the air flowed through the DW. When the damper was opened, the air bypassed the DW, decreasing the pressure drop.

Table 10: Evaporator Air Flow Profile: Damper Fully Closed

Height [mm]	**Air Velocities [m/s]**					
	Width 1	Width 2	Width 3	Width 4	Width 5	Average
127.0	1.85	1.7	1.68	1.48	1.76	1.69
193.7	1.85	1.6	1.84	1.75	1.65	1.74
260.4	1.81	1.69	1.73	1.64	2.03	1.78
327.0	1.85	1.8	1.7	1.81	1.7	1.77
393.7	1.98	1.96	1.95	1.89	2.01	1.96
Average	1.87	1.75	1.78	1.71	1.83	1.79

Table 11: Evaporator Air Velocity Profile: Damper Fully Opened

Height [mm]	Air Velocities [m/s]					
	Width 1	Width 2	Width 3	Width 4	Width 5	Average
127.0	2.50	2.61	2.79	2.7	2.55	2.63
193.7	2.53	2.41	3.02	3.3	2.86	2.82
260.4	2.58	2.71	3.11	3.37	3.6	3.07
327.0	2.77	2.81	3.09	3.15	3.5	3.06
393.7	2.66	2.65	2.92	3.08	3.31	2.92
Average	2.61	2.64	2.99	3.12	3.16	2.90

Table 10 and Table 11 show the results of the air flow testing over the evaporator for both cases of damper opened and damper closed. Immediately, the difference in average air velocity proves the difference in pressure drop due to the DW. From the velocity, the volumetric flow rate can be determined by multiplying the velocity by the surface area of the evaporator. Based on Figure 18, the performance curve of the evaporator fan, the difference in pressure drop between the two cases was 170 Pa, confirming the estimated pressure drop across the DW.

Even though there were obstructions within the path of air flow after the evaporator, the distribution of the velocity over the evaporator is relatively uniform in both cases. Due to the relatively even distribution of the evaporator, there was no need to model the distribution of the air flow.

The issue that arose when testing the air flow rate over the evaporator was the low volumetric flow rate being measured. One big issue was the alignment of the evaporator fan and the inlet nozzle ring.

Figure 67: Evaporator Fan Gap Before Adjustment

Figure 67 shows a significant gap between the fan and the inlet. What ends up happening because of the gap is the air is blowing out the fan outlet and being sucked back into the fan inlet, significantly reducing the performance of the fan. The fan duct required more precise construction that we originally intended.

Figure 68: Evaporator Fan Gap After Adjustment

Figure 68 shows the evaporator fan after adjustments were made to reduce the gap as much as possible. The duct was raised to the point just before the fan and the inlet nozzle were scrapping. The gap would still affect the performance, but now significantly less than it originally did.

Table 12 reports the results of the evaporator air flow testing before and after adjustments were made.

Table 12: Evaporator Air Flow Results

Description	Average Velocity [m/s]	Air Flow Rate [m^3/h]
Damper Closed	1.8	547
Damper Opened	2.9	889
Damper Closed (adjusted)	2.6	797

The adjustments made to the evaporator fan inlet increased the volumetric flow rate from 547 to 797 m^3/h. 797 m^3/h was below the original design point of 934 m^3/h for the air flow rate over the evaporator. Simulations were run using 797 m^3/h and the required cooling capacity was still met. The evaporator was oversized originally, allowing for the reduced air flow rate to not affect the performance of the system.

5.1.2: Desuperheat Condenser

Air Flow Testing of the desuperheat condenser was done in the same manner as the evaporator. The fan was run at full capacity and readings were taken at different points and depths immediately after the heat exchanger.

Table 13 shows the profile of the desuperheat condenser.

Table 13: Desuperheat Condenser Air Velocity Profile

Height	Air Velocities [m/s]					
	Width 1	Width 2	Width 3	Width 4	Width 5	Average
Top	1.25	1.03	1.18	1.04	0.87	1.07
Middle	1.06	1.14	1.25	1.2	1.03	1.14
Bottom	1.12	1.38	1.06	1.05	0.93	1.11
Average	1.14	1.18	1.16	1.10	0.94	1.11

Similarly to the evaporator fan, the distribution was relatively even and did not require further simulation testing to study the effects of an uneven distribution. Based on the restricted air flow path of the condenser due to the close proximity of the DW at an angle to the condenser, the relatively even distribution was extremely good.

Using the surface area and the velocity, the volumetric air flow rate across the condenser was calculated to be 325 m^3/h. Based on modeling and simulation, in order to reach the required 50°C regeneration temperature and provide enough cooling to reach the two phase region, the air flow rate needed to be between 125-170 m^3/h. The fan could be operated close to 50% of full capacity in order to meet the design point of the desuperheat condenser. Running the fan at 50% of full capacity would be a significant decrease in power consumption of the desuperheat condenser's centrifugal fan of between 20-30 W.

5.1.3: Condenser II

Air flow testing of the condenser II was also done similarly to the first two heat exchangers. In this case though, the air flow testing was done at 100% capacity as well as 75% capacity to determine if there was a difference in the distribution at different air flow rates.

Table 14 and

Table 15 show the air velocity profiles over the condenser at 100% and 75% fan capacity, respectively. There is an obvious uneven distribution of air flow in both cases, both centering on a lower flow rate at the center of the profile. This can be

attributed to the desuperheat centrifugal fan directly in the air flow path of the condenser which can be seen in Figure 60.

Table 14: Condenser II Air Velocity Profile at 100% Fan Capacity

Height	Air Velocities [m/s]					
	Width 1	Width 2	Width 3	Width 4	Width 5	Average
Top	6.1	4.2	2.8	2.9	5.5	4.3
Middle	4.5	2.5	2.4	2.5	3.9	3.2
Bottom	5.2	4.7	4.9	3.9	4.3	4.6
Average	5.3	3.8	3.4	3.1	4.6	4.0

Table 15: Condenser II Air Velocity Profile at 75% Fan Capacity

Height	Air Velocities [m/s]					
	Width 1	Width 2	Width 3	Width 4	Width 5	Average
Top	5.2	3.6	2.4	2.6	4.5	3.7
Middle	3.6	2.3	1.9	2.3	2.8	2.6
Bottom	4.4	3.6	4.1	2.9	3.5	3.7
Average	4.4	3.2	2.8	2.6	3.6	3.3

Table 16 shows the results using the average velocity over the entire heat exchanger. Even with the significant mal-distribution, the design point flow rate is surpassed at 75% fan capacity. This means that in full operation, the condenser fan can run closer to 65-70% of full capacity, decreasing the power consumption of this fan as well.

Table 16: Condenser II Air Flow Results

Exhaust Condenser II Fan Capacity	Average Velocity [m/s]	Air Flow Rate [m^3/h]
100%	4.0	1,640
75%	3.3	1,350

Even though the average velocity met the requirements for meeting the condenser capacity, the uneven distribution could have adverse effects on the capacity. The uneven distribution was modeled in CoilDesigner to see what the effect on the condenser capacity would be.

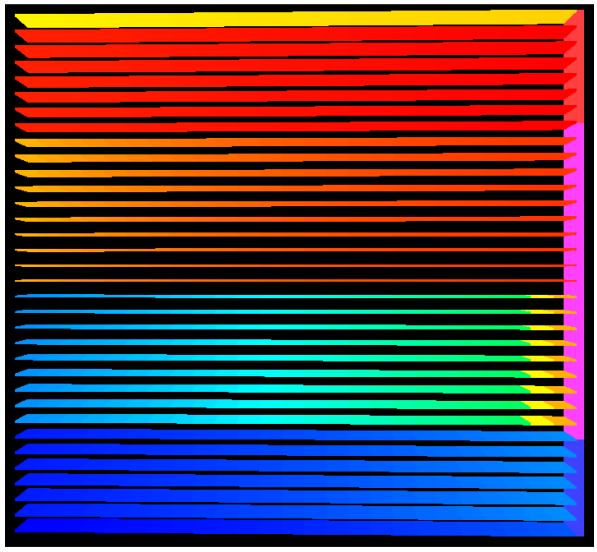

Figure 69: Outlet Air Temperature Profile of Condenser with Evenly Distributed Inlet Conditions as Modeled In CoilDesigner

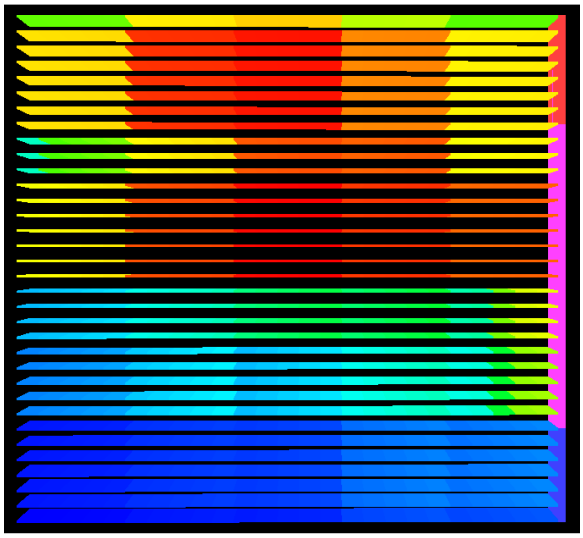

Figure 70: Outlet Air Temperature Profile of Condenser with Non-Evenly Distributed Inlet Conditions Based on Experimental Results as Modeled In CoilDesigner

Figure 69 shows the condenser modeled in coil designer with a standard even distribution of air over the heat exchanger. Figure 70 shows the condenser experimental results modeled in CoilDesigner in order to determine the effects of the uneven distribution of airflow on the capacity of the condenser.

The capacity of the evenly distributed model was 2,700 W of heat removal. The capacity of the experimental results modeled in CoilDesigner as an uneven distribution was 2,688 W of heat removal. There was a negligible difference in the capacity due to the uneven distribution of air flow. Therefore, no changes needed to be made to the system to fix the uneven distribution. Points along the condenser where air flow was too low were made up for at points where the velocity was much higher. Even though certain parts of the condenser were not receiving the cooling other parts were, or even the average cooling, it did not affect the capacity of the condenser.

5.2: Vapor Compression Cycle Testing

Shakedown testing was done on the refrigeration system in order to get baseline results and study the effects of the components changes made to the system, specifically the MCHX and the high evaporator inlet temperature. It was also important to test the capabilities of the fans and determine the required operation point of each of the three fans for optimum efficiency of the VCS separately.

5.2.1: System Performance

The system was run according to AHRI standard 310 [8]. Adjustments were made to the system during shakedown testing in order to optimize the system. Figure 71 shows the P-h diagram of the VCC during testing.

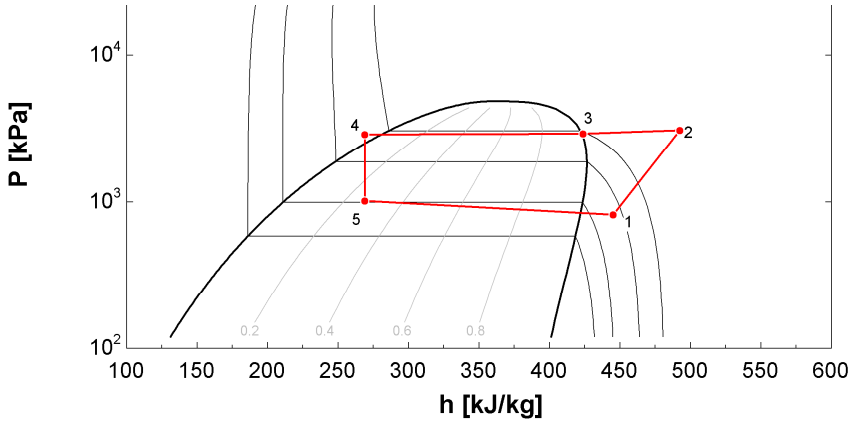

Figure 71: VCC in P-h Diagram

Table 17: VCC State Point Results

State Points	Comp. Suction	Comp. Discharge	Cond. sat.v-Cond. sat.l	Cond. Outlet	Evap. Inlet
Temperature [°C]	15.7	84.0	47.3	44.4	13.9
Pressure [kPa]	965.0	3,087.9	2,839.7	2,807.9	1,218.2

Table 17 shows the state points of the VCC. During testing, the high evaporation inlet temperature was lower than the dew point temperature, causing a latent load through the evaporator. The compressor discharge temperature was similar to the simulated value, allowing for the desuperheat air temperature to reach the required minimum regeneration temperature.

Table 18: VCC Summary of Results

Variable	Unit	Value	Variable	Unit	Value
Superheat	°C	9.6	Refrigerant Mass Flow Rate	g/s	18.8
Subcooling	°C	1.4	Evaporator Capacity (Ref.)	kW	2.97
Air Flow Rate	m^3/h	816	Evaporator Capacity (Air)	kW	3.27
Compressor Power	W	935	Energy Balance	%	8.5

Table 18 summarizes the results from the VCC testing. The evaporator capacity on the refrigeration side was measured during testing using the temperatures, pressures and mass flow rate of the system and was determined to be 2.97 kW. The air side evaporator capacity was calculated higher at 3.27 kW based on the air flow rate calculated using the heater and pre and post heater temperatures. The energy balance between the capacities was 8.5%. The compressor power input was higher than the VCC simulation. The increase in compressor power was due to the significantly large pressure drops through the MCHX's which will be discussed further in the next section. The refrigerant mass flow rate was similar to the simulated value, allowing for the capacity to reach a higher value, but with greater compressor power consumption. The actual capacity of the system is most likely closer to the refrigerant side capacity rather than the air side capacity due to the lower uncertainty associated with the refrigeration instrumentation.

Table 19: Heat Exchanger Pressure Drop

Heat Exchanger	Pressure Drop [kPa]
Evaporator	253.2
Desuperheat Condenser	248.2
Condenser II	31.9

The pressure drop over each MCHX was calculated and summarized in Table 19. The pressure drops through the evaporator and desuperheat condenser were

higher than expected, causing an increase in compressor power consumption. Originally, the evaporator pressure drop was double the reported value, but an additional evaporator was connected in parallel to reduce the pressure drop and increase the capacity of the system. Although the addition of the second parallel evaporator decreased the pressure drop, 253 kPa was still an unreasonable high value for the low side pressure drop.

The desuperheat condenser is identical in design to the evaporator, but matches the pressure drop due to the refrigerant being in the vapor phase through the condenser. The condenser II pressure drop is much more reasonable at 31 kPa due to the larger design as well as the refrigerant mainly in the two-phase region throughout most of the heat exchanger. A more reasonable value in pressure drop would be 50 kPa for the evaporator and 100 kPa for both condensers combined, allowing for closer to 70 kPa pressure drop through the desuperheat condenser. By reducing the total pressure drop by 60% the compressor power will significantly decrease and increase the overall COP of the system. The MCHS's would need to be redesigned to optimize the pressure drop through them.

5.3: Regeneration Air Loop

Table 20: Desuperheat Condenser Air Temperature Distribution

Thermocouple Position	Temperature [°C]
Top	63.8
Middle	50.4
Bottom	46.2
Average	53.5

Table 20 shows the distribution of the air flow temperature across the desuperheat condenser. Because the refrigerant is superheated in the vapor region in this condenser, there is a significant temperature drop, creating the distribution seen in the table. The average air temperature meets the regeneration temperature requirement of 50°C, but due to a lack of mixing after the condenser, there could still be an issue with regeneration on the lower portion of the DW. Also, the extremely high top temperature could add to the heat load on the process air side, reducing the cooling capacity of the system. The air flow rate through the DW is still too high, causing the lower bottom temperature value. The air flow rate needs to be reduced by half, which could pull the bottom temperature above the required regeneration temperature. Decreasing the flow rate would also increase the temperature of the top portion of the condenser though, adding a larger heat load to the process air. A balance needs to be struck between the heat load and the regeneration temperature.

A possible solution would be to redesign the desuperheat condenser into a single pass MCHX which would more evenly distribute the temperature profile of the heat exchanger. This solution would also reduce the pressure drop through the condenser.

5.4: Process Air Loop

Table 21 shows the results of the process air state points. The temperature and relative humidity were measured before the evaporator, after the evaporator and at the outlet of the system after the fan.

Table 21: Process Air Side Results

Variable	Unit	Evaporator	Evaporator	Process Air

		Inlet	Outlet	Outlet
Temperature	°C	26.6	12.3	22.8
Relative Humidity	%	49.38	92.81	49.33
Humidity Ratio	g/kg	10.77	8.23	8.50

The decrease in humidity ratio at the evaporator outlet show that there is a latent load associated with the evaporator. This was due to the evaporator inlet temperature remaining above the dew point temperature of the air. The system still needs to be optimized for sensible only cooling, which would be validated when the humidity ratio before and after the evaporator are equal.

The process air outlet shows a slight increase in the humidity ratio which could be caused by two different factors. The first factor is the high uncertainty associated with the relative humidity sensors. The sensors used were high quality sensors, but still had an accuracy of ±1% relative humidity, which only increases as the relative humidity increases as it does immediately after the evaporator. The other factor that could actually be increasing the humidity ratio is the condensed moisture from the latent cooling on the evaporator. The moisture is sitting in the system which could be absorbed by the air later in the process again. During standard operation of the SSLC system, this would not be an issue, but during the tested conditions, it was due to the lower than desired evaporator temperature.

Another issue seen in Table 21 is the process air outlet. Most of the sensible cooling done is lost before the air leaves the system. The main contributing factor was the lack of insulation inside and outside the system. The wall separating the process and airside flows could be acting as a heat exchanger, so insulating that barrier would immediately decrease some of the heat exchange between the evaporator and condenser side air loops. There is also a lack of insulation outside of

the main system before the thermocouple grid measuring the outlet air temperature. The duct is subject to the ambient temperature, most likely increasing the process air temperature as well. An increase in temperature is expected as the air flows through the DW and process air side loop, but a 10°C temperature increase may not be justified and needs further investigation. .

Chapter 6: Conclusions

A PTAC type DW assisted SSLC system was designed, constructed, and tested for manufacturing purposes. The system was the second iteration in SSLC air conditioning units. In order to produce a marketable product, certain objectives had to be met in order to keep the size and cost down, and the energy reduction benefits up. The system was modeled after PTAC type AC units currently on the market as the smallest size AC unit that could integrate the solid DW.

The SSLC system provides a more efficient AC unit, with lower annual costs to the consumer, as well as increased thermal comfort. By separating the sensible and latent cooling, the desired thermal comfort point can be reached without wasting energy. The DW reutilizes the waste heat from the VCC, adding the additional latent load at a negligible addition to the power consumption.

The test facility was constructed in order to measure the cooling capacity of the SSLC system, as well as monitor the refrigeration and air side loops within the system. Because of the emphasis on the latent load, humidity and temperature were extremely important properties of the air side loops. Because the VCC was required to operate as a purely sensible load system, more precise control of the refrigerant state points was also necessary. The test facility consisted on the main system,

designed to fit within the restricted size limitations of a standard PTAC unit, and the process air side duct, representing the space conditions during normal operation.

Because the combined SSLC system is newer technology, each component requires constant optimization as testing continues. Certain components such as the MCHX's were optimized but as testing progressed certain aspects were more important such as the pressure drops, the even temperature distribution over the desuperheat condenser, or the high evaporator inlet temperature. The realizations made during testing required parts of the system to be sent back to the design phase, but that only increases the optimization of this new technology. Each set back is a lesson learned widening the knowledge and understanding of SSLC systems.

Further optimization and testing of the SSLC PTAC unit must be done in order to reach the objectives set for the project. The point the system is at currently is not far from reaching its full potential, but must be altered in order to assure maximum efficiency increase and power savings over the standard VCC AC units currently on the market today.

Chapter 7: Future Work

The data collected thus far from the SSLC PTAC unit has been useful in optimizing the system. Certain component designs did not perform as simulated or modeled which is expected for such novel experimental commercial prototype design. Each test of the system provided information on what still needed to be done in order to optimally run the system.

The first major change that needs to be made is the redesign of the heat exchangers. The MCHX's were chosen as more compact and efficient options over standard tube-and-fin coils. However, the refrigerant side pressure drop was much higher than expected, reducing the efficiency of the system through a substantial increase in compressor power consumption. Once the heat exchangers are redesigned and replaced and an optimized VCC is installed, a more accurate understanding of the benefits of the addition of the DW would be highlighted.

Because of the current VCC, the system cannot currently perform in an SSLC mode. The evaporator must be a solely sensible coil, to remove excess moisture from the system, and allow for the DW to remove the full latent load. In addition, the test facility must be insulated better in order to reduce cooling capacity lost to the environment.

In order to properly regenerate the DW, a variable speed fan must replace the current desuperheat condenser fan. This will allow the system to reach the design point regeneration temperature, as well as decrease the fan power consumption, giving the system more accurate total power consumption.

Once those changes are made, the system can be tested and the air flow and latent capacity through the DW can be optimized by making adjustments to the air flow bypass as well as the rotational speed of the DW. After the system meets its desired capacity, with a full understanding of all measurements within the system such as pressure drops, air flow rates and operating temperatures, the fans and compressor can be more specifically sized to reduce power consumption and increase the efficiency further.

Finally, with all of the results collected at the optimal test point, a better understanding of the market potential of the system can be made. A more accurate cost of the entire system can be pinpointed based on specific components chosen to minimize cost and consumption, and maximize capacity. Testing under different conditions will also provide a better understanding of how the unit will operate in different regions, and as well as a better understanding of how the system can be improved further. Manufacturing and marketing is the end goal of the DW assisted SSLC system, in order to replace the current PTAC units with a more efficient, more cost effective and more convenient system of the future.

References

[1] J. Ling, "Energy Savings and Thermal Comfort of Separate Sensible and Latent Cooling Air-Conditioning Systems," University of Maryland, College Park, MD, 2011.

[2] M. Siemann, "Separate Sensible and Latent Cooling Air Conditioner using Radiative Cooling Wall and Low Regeneration Temperature Desiccant," Department of Mechanical Engineering, University of Maryland, College Park, MD 2012.

[3] F-Chart Software, *Engineering Equation Solver (EES)*, Madison, WI, < http://www.fchart.com/ees/>.

[4] Center for Environmental Energy Engineering, 2011, *CoilDesigner*, University of Maryland, < http://ceee.umd.edu/isoc/tools/coildesigner.html >.

[5] Center for Environmental Energy Engineering, 2011, *VapCyc*, University of Maryland, < http://ceee.umd.edu/isoc/tools/vapcyc.html >.

[6] Richardson, D. H., Jiang, H., Lindsay, D., and Radermacher, R., 2002, *Optimization of Vapor-Compression Systems Via Simulation*, 2002 International Refrigeration and Air Conditioning Conference, Purdue University, West Lafayette, IN, USA, July 16-19, 2002.

[7] Richardson, D. H., Aute, V., Winkler, J., and Radermacher, R., 2004, *Numerical Challenges in Simulation of a Generalized Vapor Compression Refrigeration System*, 2004 International Refrigeration and Air Conditioning Conference, Purdue University, West Lafayette, IN, USA, July 12-15, 2004.

[8] ANSI/AHRI, "Standard 310/380-2004 – Standard for Packaged Terminal Air-Conditioners and Heat Pumps," Air-Conditioning, Heating and Refrigeration Institute (AHRI), Arlington, VA, 2004.

[9] NMB Technologies Corporation, "F250 (Ø250 X 99L)," Chatsworth, CA, 2010 < http://www.nmbtc.com/pdf/fans/impellers/f250.pdf>.

[10] ebm-papst Inc., "Compact Fans for AC and DC," Farmington, CT, 2011. < http://www.ebmpapst.us/media/content/products/downloads/Compact_fans_for_AC_and_DC__2011.pdf>.

[11] ebm-papst Inc., "EC axial compact fan," Farmington, CT, 2010 < http://www.onlinecomponents.com/datasheet/w1g250hh6752.aspx?p=12 10 4268&Resource=1>.

[12] SolidWorks Corp., 2014, *SolidWorks 3D CAD*, Dassault Systems, < http://www.solidworks.com/sw/products/3d-cad/solidworks-3d-cad.htm>.